



**COUPLING OF HELMHOLTZ RESONATORS TO IMPROVE ACOUSTIC  
LINERS FOR TURBOFAN ENGINES AT LOW FREQUENCY**

**By: Dr. L. W. Dean**

**Pratt & Whitney Aircraft Division  
United Technologies Corporation**

(NASA-CR-134912) COUPLING OF HELMHOLTZ  
RESONATORS TO IMPROVE ACOUSTIC LINERS FOR  
TURBOFAN ENGINES AT LOW FREQUENCY (Pratt and  
Whitney Aircraft) 66 p HC \$4.50 CSCL 21E

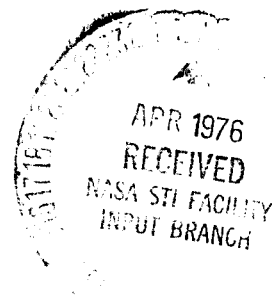
**N76-21210**

**Unclas  
G3/07 25854**

**Prepared for**

**NATIONAL AERONAUTICS AND SPACE ADMINISTRATION**

**NASA Lewis Research Center  
Contract NAS3-18552**



**JAN 29 REC'D**

1. Report No. NASA-CR-134912		2. Government Accession No.		3. Recipient's Catalog No.	
4. Title and Subtitle COUPLING OF HELMHOLTZ RESONATORS TO IMPROVE ACOUSTIC LINERS FOR TURBOFAN ENGINES AT LOW FREQUENCY				5. Report Date August 1975	
				6. Performing Organization Code	
7. Author(s) Dr. L. W. Dean				8. Performing Organization Report No. PWA-5311	
9. Performing Organization Name and Address Pratt & Whitney Aircraft Division United Technologies Corporation East Hartford, Connecticut 06108				10. Work Unit No.	
				11. Contract or Grant No. NAS3-18552	
12. Sponsoring Agency Name and Address National Aeronautics and Space Administration Washington, D. C. 20546				13. Type of Report and Period Covered Contractor Report	
				14. Sponsoring Agency Code	
15. Supplementary Notes Project Manager, Dr. Edward J. Rice, VSTOL and Noise Division, NASA-Lewis Research Center, Cleveland, Ohio					
16. Abstract <p>An analytical and test program was conducted, under NASA sponsorship, to evaluate means for increasing the effectiveness of low frequency sound absorbing liners for aircraft turbine engines. Three schemes for coupling low frequency absorber elements were considered in this program. These schemes were analytically modeled and their impedance was predicted over a frequency range of 50 to 1000 Hz. An optimum and two off-optimum designs of the mos. promising, a parallel coupled scheme, were fabricated and tested in a flow duct facility. Impedance measurements were in good agreement with predicted values and validated the procedure used to transform modeled parameters to hardware designs. Measurements of attenuation for panels of coupled resonators were consistent with predictions based on measured impedance. All coupled resonator panels tested showed an increased in peak attenuation of about 50% and an increase in attenuation bandwidth of one one-third octave band over that measured for an uncoupled panel. These attenuation characteristics equate to about 35% greater reduction in source perceived noise level (PNL), relative to the uncoupled panel, or a reduction in treatment length of about 24% for constant PNL reduction. This program demonstrated the increased effectiveness of the coupled resonator concept for attenuation of low frequency broad spectrum noise.</p>					
17. Key Words (Suggested by Author(s)) Muffler Coupled Resonators Helmholtz Resonators Acoustic Treatment			18. Distribution Statement		
19. Security Classif. (of this report) Unclassified		20. Security Classif. (of this page) Unclassified		21. No. of Pages	22. Price*

\* For sale by the National Technical Information Service, Springfield, Virginia 22151

## TABLE OF CONTENTS

Section	Title	Page
	SUMMARY	1/2
1.0	INTRODUCTION	3/4
1.1	Background	3/4
1.2	Program	3/4
2.0	ANALYTICAL STUDIES	5
2.1	Approach Used in Modeling Resonators	5
2.1.1	Analytical Modeling of Single Resonator Impedance	7
2.1.2	Analytical Modeling of Coupled Resonator Impedance	10
2.1.2.1	Series Coupled Resonators	12
2.1.2.2	Parallel Coupled Resonators	14
2.1.2.3	Folded Coupled Resonators	15
2.1.3	Analytical Attenuation Calculations	16
2.2	Liner Optimization	17
2.2.1	Optimization Criteria for Uncoupled and Coupled Resonators	19
2.2.2	Alternate Optimization Criterion	19
2.3	Selection of Coupled Resonator Configurations for Test	20
2.3.1	Series Coupled Resonator	21
2.3.2	Parallel Coupled Resonator	22
2.3.3	Folded Coupled Resonator	23
2.3.4	Selection of Most Promising Scheme	24
2.3.5	Definition of the Optimum Parallel Coupled Resonator Configuration	26
2.3.6	Definition of Two Off-Optimum Parallel Coupled Resonator Configurations	28
2.4	Analytical Evaluation of Coupled Resonators	28
2.4.1	Baseline and Improved Baseline Attenuation Predictions	29
2.4.2	Optimum and Off-Optimum Coupled Resonator Panel Predicted Attenuation	30
2.4.3	Analytical Evaluation of the Coupled Resonator Concept	30
3.0	TEST PROGRAM	34
3.1	Resonator Impedance Tests	34
3.1.1	Impedance Test Facility	34
3.1.2	Uncoupled Resonator Measured Impedance and Comparison with Predicted Values	37

**TABLE OF CONTENTS (Cont'd)**

Section	Title	Page
	3.1.2.1 Effect of Resonator Geometry	37
	3.1.2.2 Effect of Grazing Flow	41
	3.1.2.3 Effect of Sound Pressure Level	42
	3.1.3 Coupled Resonator Impedance Measurements	42
	3.1.4 Comparison of Coupled Resonator Impedance Measurements with Predicted Values	44
3.2	Coupled Resonator Attenuation Test Results	48
	3.2.1 Coupled Resonator Attenuation Test Facility	48
	3.2.2 Comparison of Predicted and Measured Attenuation of Coupled Resonator Panels	48
3.3	Evaluation and Improvement of Resonator Models	51
3.4	Evaluation of the Coupled Resonator Concept	54
	3.4.1 Evaluation on Basis of Alternate Criterion	56
4.0	CONCLUSIONS AND RECOMMENDATIONS	58
	4.1 Conclusions	58
	4.2 Recommendations	58
LIST of SYMBOLS		59
REFERENCES		60

## LIST OF ILLUSTRATIONS

		<u>Page No.</u>
Figure 2-1	Diagram of Resonator Modeling Process	6
Figure 2-2	Comparison of Single Resonator Impedance Model with Measured Data, Uncoupled Resonator # 3	10
Figure 2-3	Resonator Coupling Schemes	11
Figure 2-4	Predicted Impedance for a Series Coupled Resonator	13
Figure 2-5	Contours of Constant Attenuation in the Impedance Plane, $M_n = 0.45$ , Least Attenuated Mode	17
Figure 2-6	Optimum Resistance and Reactance for Sample Uncoupled Resonator, $M_n = 0.45$	18
Figure 2-7	Low Frequency Core Noise Spectrum	20
Figure 2-8	Comparison on an Annoyance Basis of Predicted Performance of the Three Coupling Schemes	25
Figure 2-9	Parallel Coupled Resonator Geometric Parameters	27
Figure 2-10	P&WA Baseline Resonator	29
Figure 2-11	Comparison of Predicted Coupled Resonator Attenuation, $M_n = 0.45$	31
Figure 2-12	Comparison of Predicted Effects of Coupled Resonators on Source Spectrum in Annoyance Units, $M_n = 0.45$	31
Figure 2-13	Comparison of Predicted Attenuation for Coupled and Uncoupled Baseline Resonators, $M_n = 0.45$	32
Figure 2-14	Comparison of Predicted Effects of Coupled and Uncoupled Baseline Resonators on Source Spectrum in Annoyance Units, $M_n = 0.45$	32
Figure 3-1	Flow Duct Facility	34
Figure 3-2	Impedance Data System	35
Figure 3-3	Microphone Placement for Uncoupled Resonator Impedance Measurements	36

## LIST OF ILLUSTRATIONS (Cont'd)

Figure 3-4	Comparison of Predicted and Measured Impedance, Resonator #1 at $M_n = 0.45$	38
Figure 3-5	Comparison of Predicted and Measured Impedance, Resonator #2 at $M_n = 0.45$	39
Figure 3-6	Comparison of Predicted and Measured Impedance, Resonator #3 at $M_n = 0.45$	40
Figure 3-7	Comparison of Predicted and Measured Impedance, Resonator #1 at $M_n = 0.27$	41
Figure 3-8	Microphone Placement for Coupled Resonator Impedance Measurements	43
Figure 3-9	Comparison of Predicted and Measured Impedance, Off-Optimum A Coupled Resonator at $M_n = 0.45$	44
Figure 3-10	Comparison of Predicted and Measured Impedance, Optimum Coupled Resonator at $M_n = 0.45$	45
Figure 3-11	Comparison of Predicted and Measured Impedance, Off-Optimum B Coupled Resonator at $M_n = 0.45$	46
Figure 3-12	Coupled Resonator Impedance Data at $M_n = 0.27$	47
Figure 3-13	Comparison of Attenuation Predicted from Model and Measured Impedance, Optimum Configuration at $M_n = 0.45$	48
Figure 3-14	Comparison of Predicted and Measured Attenuation for Three Coupled Configurations, $M_n = 0.45$	49
Figure 3-15	Comparison of Three Coupled Configurations on an Annoyance Basis	50
Figure 3-16	Comparison of Measured Attenuation for Baseline and Optimum Coupled Configuration at $M_n = 0.45$	51
Figure 3-17	Comparison of Calculated and Measured Coupled Resonator Impedance, Off-Optimum A, $M_n = 0.45$	52
Figure 3-18	Comparison of Calculated and Measured Coupled Resonator Impedance, Optimum, $M_n = 0.45$	53

**LIST OF ILLUSTRATIONS (Cont'd)**

Figure 3-19	Comparison of Calculated and Measured Coupled Resonator Impedance, Off-Optimum B, $M_n = 0.45$	54
Figure 3-20	Source Spectrum PNL Reduction Versus Reciprocal of Degrees of Freedom	56

## LIST OF TABLES

Table	Title	Page No.
2-I	Optimum Resistance and Reactance for Typical Mach Numbers and Frequencies	19
2-II	Attenuation of Various Series Coupled Configurations	22
2-III	Attenuation of Various Parallel Coupled Configurations	23
2-IV	Attenuation of Various Folded Coupled Configurations	24
2-V	Optimum Parameters for Parallel Coupled Configurations	27
2-VI	Summary of Coupled Resonator Design Parameters	28
2-VII	Baseline Resonator Parameters, $M_n = 0.45$	30
2-VIII	Predicted PNL Reduction of Source Spectrum Achieved by 50.8 cm of Baseline and Coupled Resonators, $M_n = 0.45$	33
3-I	Uncoupled Resonator Geometrical Parameter Values	37
3-II	Summary of Resonator Attenuation on PNL Basis, 50.8 cm Length, $M_n = 0.45$	50
3-III	Equivalent Lengths of Coupled and Baseline Liners for Source Reduction of 3.8 PNdB, $M_n = 0.45$	57

## SUMMARY

The objective of the work conducted under this contract was to evaluate means for increasing the effectiveness of low frequency sound absorbing liners for aircraft engines by coupling low frequency absorber elements, such as Helmholtz resonators. While single, uncoupled Helmholtz resonators are very effective absorbers for a pure tone acoustic spectrum, they do not represent the most effective device for attenuation of broad spectrum noise in that the impedance characteristics can be designed to be optimum only in the vicinity of a single frequency. The concept of coupling resonators results in an absorbing liner with more adjustable parameters, or degrees of freedom, that can be tailored to be more nearly optimum over a range of frequency and more suitable to attenuate broad spectrum noise. Specifically the problem of attenuation of low frequency core engine noise is considered requiring an absorber that is effective over a frequency range of one to two octaves centered at 400 Hz.

Three schemes for coupling resonators in pairs were modeled analytically and studied to determine the most promising. All comparisons were made holding total attenuating liner volume constant and equal to that of a baseline uncoupled resonator absorber previously evaluated by P&WA. The most promising coupling scheme was found to be one in which the resonator pairs were coupled in parallel.

The parallel coupled scheme was optimized by varying the design parameters to minimize the perceived noise level (PNL) of a typical low frequency core engine spectrum. An optimum and two off-optimum designs were defined, and the designs were translated into hardware with the aid of results of tests on single uncoupled resonators aimed at relating resonator design parameters to resonator geometry, grazing flow, and sound pressure level.

Measurements of impedance of the optimum and off-optimum coupled resonators were made and were found to be in good agreement with predictions based on the governing equations. It was concluded that the transformation of the coupled designs to hardware was accomplished satisfactorily.

Measurements of attenuation of panels of coupled resonators were in agreement with predictions based on measured impedance. Furthermore, all coupled resonator panels tested showed an increase in peak attenuation of about 50% and an increase in attenuation bandwidth of one one-third octave band over that obtained for the P&WA supplied uncoupled resonator panel. These improvements in attenuation characteristics resulted in source spectrum PNL reduction about 35% greater for the coupled resonator panel than for the equal length of uncoupled baseline treatment. Alternately it was determined that the coupled resonator treatment length could be reduced by 24% and provide the same PNL reduction as the tested length of uncoupled baseline treatment. The coupled resonator concept, therefore, was determined to represent a significant improvement in treatment effectiveness over the single uncoupled concept for attenuation of low frequency broad spectrum noise.

## 1.0 INTRODUCTION

### 1.1 BACKGROUND

Low frequency noise is generated in the core engine section of modern turbofan engines, and is predicted to be a significant noise source from future high bypass ratio engines. For example, core engine noise has been identified as an area of concern for the JT8D-109 Refan engine being studied under a NASA contract. Unpublished estimates indicate that the noise characteristics of this engine could be improved significantly, by a 2 to 4 dB reduction of low frequency core engine noise. For current high bypass engines in acoustically treated nacelles, such as are used to power the 747, DC-10 and L1011, it has been estimated that core noise is within 5 EPNdB of the noise level set by the fan<sup>(1)\*</sup>. Consequently, core noise suppression will be required for future models of these airplanes if significantly lower noise levels are to be achieved.

Because earlier turbofan engines were fan noise dominated, acoustic treatment technology evolved for the frequency range above 2000 Hz where prominent fan tones clearly were identified. Following the successful inflight demonstrations of acoustically treated nacelles conducted by NASA in 1969 using 707<sup>(2)</sup> and DC-8<sup>(3)</sup> aircraft, acoustic treatment has been incorporated in fan inlets and fan ducts of a variety of production airplanes. Although further high frequency fan noise attenuation can be achieved, low frequency core engine noise may limit the benefits that can be realized. Consequently, technology must be developed to suppress core engine noise. Pratt & Whitney Aircraft was awarded a contract (NAS3-18552) to conduct an Advanced Acoustics Suppression Concepts program to develop low frequency acoustic treatment technology.

### 1.2 PROGRAM

The objective of this program was to evaluate means for increasing the effectiveness of low frequency sound absorbing liners by coupling low frequency absorber elements, such as Helmholtz resonators or folded deep backing depth liners, to achieve higher attenuation over a broader frequency range. The technical effort under this program was accomplished in two phases: detailed analytical studies of selected concepts, and an experimental program to test configurations identified as most promising under the analytical studies.

The analytical studies consisted of development of analytical models of three coupled low frequency absorber element configurations and selection of the most promising for testing. This study also included development of prediction procedures for resonator impedance and attenuation, and definition of configurations for test model fabrication. The test program was conducted in the P&WA dual reverberation chamber flow duct facility. Impedance measurements were taken on single resonators and the coupled resonators, defined during the analytical studies, at three values of grazing flow velocity for two sound pressure levels over a range of frequencies from 50 to 1000 Hz. The results of these tests were used to verify and improve the impedance models. Attenuation spectra were obtained for the three coupled resonator configurations for a low frequency broadband noise source at three values of grazing flow (Mach number (Mn) 0, 0.27, and 0.45) and one value of overall sound pressure level (140 dB) typical of core levels.

\*Note: A list of references is provided on page 60.

## 2.0 ANALYTICAL STUDIES

### 2.1 APPROACH USED IN MODELING RESONATORS

Analytical models of the coupled resonators were developed to provide the basic tools for predicting impedance and attenuation characteristics of the three coupling schemes. In particular, predictions from the models were used in the optimization of the three coupling schemes, the selection of the most promising, and the definition of an optimum and two off-optimum configurations for test. In this section, the approach used to model the resonators will be described. Detailed descriptions for each particular resonator type considered are included in subsequent sections.

In all cases, lumped parameter modeling was employed and the models were constructed in terms of the analogous impedance\* of the individual physical elements<sup>(4)</sup>. The condition under which lumped parameter modeling is useful, that the physical dimensions of the resonators be less than a quarter wavelength of sound over the frequency range of interest, is satisfied over most of the test frequency range, 50 to 1000 Hz, inasmuch as the largest resonator dimension is 10 cm and the smallest acoustic wavelength of interest is 34 cm (at 1000 Hz).

The modeling process for both single and coupled resonators consists of the two steps diagrammed schematically in Figure 2-1. As indicated, the first step consists of a derivation of the impedance by using the equations of motion applied to a lumped parameter representation of the Helmholtz resonators. The equations of motion are expressed in the time domain, and the lumped parameters, which form the coefficients in the resulting differential equations, are taken to be constants. Impedance, the quantity that is to be the end product of the modeling, is defined in the frequency domain and is obtained by assuming the dependent variables to vary sinusoidally with time.

\*Note: The term "analogous impedance" is taken from Reference (4), *Vibration and Sound* by P.M. Morse. In this text, lumped parameter modeling of acoustic devices, including resonators, is developed in terms of electric circuit analogies. Voltage is conveniently analogous to pressure and current to volume velocity (velocity times area). Correspondingly, the analogous impedance in acoustic quantities is the ratio of pressure to volume velocity. The *acoustic* impedance is defined as the ratio of pressure to *velocity* and is equal to the analogous impedance multiplied by an appropriate area.

The lumped parameters are masses associated with necks or constrictions ( $M_i$ ), resistances associated with dissipative elements ( $R_i$ ), and spring constants associated with enclosed volumes ( $C_i$ ) of the resonator or resonator arrays. In the second step in the modeling process indicated in Figure 2-1, these parameters are determined in terms of resonator geometry, grazing flow, applied sound pressure level, and the ambient properties of the medium by measuring impedance and inferring their values from the equation for impedance (see Section 3.1). The measured resistance parameter of a single resonator with grazing flow, as discussed in the next section, is found to be a function of frequency. In the modeling, the function is approximated by a constant. This approximation permits the description of the single resonator with flow as a simple harmonic oscillator with a viscous damping term identified with the resonator neck. Improvements on this model are discussed in Section 3.3.

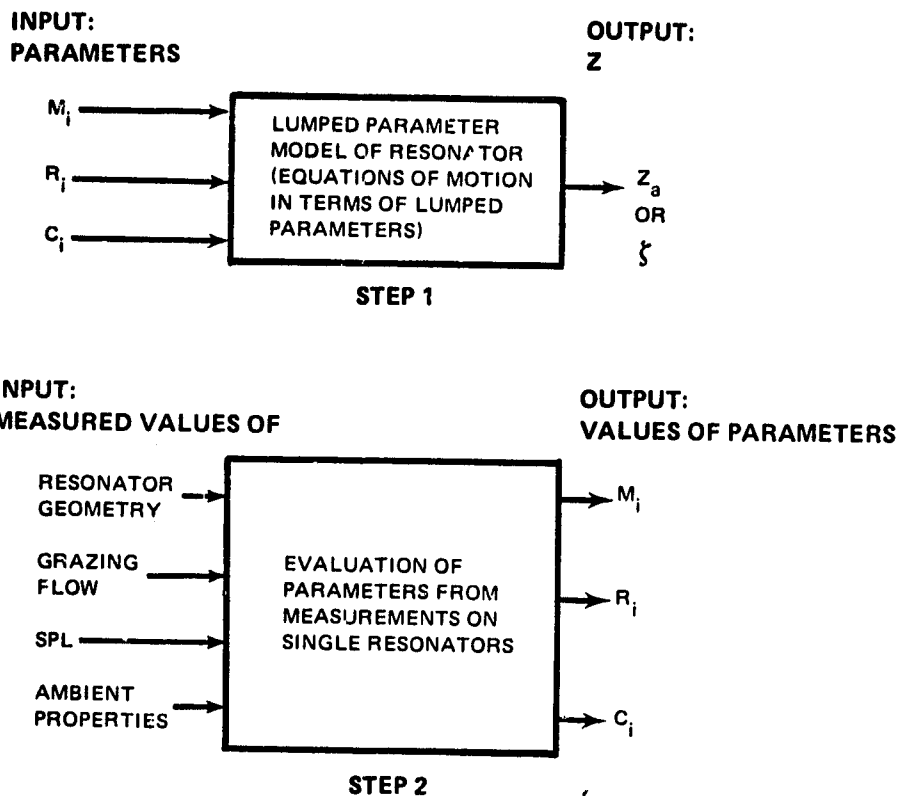


Figure 2-1 Diagram of Resonator Modeling Process

Through the equations of motion, the volume velocity at a resonator neck is related to the applied pressure by the analogous impedance (in the frequency domain). The quantity useful subsequently to calculate attenuation, however, is the ratio of applied pressure to the *average velocity* normal to the surface of the resonator. The non-dimensional form of this ratio, the *specific acoustic impedance*, is the end result of most of the calculations, and the two impedances are related by the equations:

$$\zeta = \theta + i\chi = Z_a A_s / \rho_0 c \quad 2-1$$

where

$\zeta$  = specific acoustic impedance

$\theta$  = specific acoustic resistance

$i = \sqrt{-1}$

$\chi$  = specific acoustic reactance

$Z_a = R_a + iX_a$  = analogous impedance (cgs Rayls/cm<sup>2</sup>)

$R_a$  = analogous resistance (cgs Rayls/cm<sup>2</sup>)

$X_a$  = analogous reactance (cgs Rayls/cm<sup>2</sup>)

$A_s$  = resonator surface area (cm<sup>2</sup>)

$\rho_0$  = ambient density (g/cm<sup>3</sup>)

$c$  = ambient speed of sound (cm/sec)

This notation will be used consistently throughout this report.

### 2.1.1 Analytical Modeling of Single Resonator Impedance

The resonator modeling procedure outlined in the previous section is most conveniently explained in terms of single uncoupled resonators because of the basic simplicity of the system. Models corresponding to the two steps in Figure 2-1 for single resonators were taken from the literature<sup>(4, 5, and 6)</sup> and from previous P&WA experience with resonator duct liners at higher frequencies (1,000 to 10,000 Hz).

The empirical equations that result for the analogous resistance and reactance of a resonator exposed to flow are:

$$R_a = a_1 M n \rho_0 c / A_h \text{ (gm/cm}^4 \text{ sec)} \quad 2-2$$

$$X_a = \left( \frac{\rho_0 l_e}{A_h} \right) \omega - \left( \frac{\rho_0 c^2}{V} \right) \frac{1}{\omega} = M_a \omega - \frac{1}{C_a \omega} \quad 2-3$$

where

$\omega$  = angular frequency

$a_1$  = an experimentally derived constant

$M_n$  = (free stream) grazing flow Mach number

$A_h$  = resonator neck cross sectional area ( $\text{cm}^2$ )

$l_e$  = effective length of the resonator neck (cm)

$V$  = enclosed volume ( $\text{cm}^3$ )

$M_a$  = analogous mass ( $\text{gm}/\text{cm}^4$ )

$C_a$  = analogous capacitance or compressability ( $\text{cm}^4 \text{sec}^2/\text{gm}$ )

These expressions were derived from the equation of motion for a Helmholtz resonator, i.e.,

$$M_a \frac{dq}{dt} + R_a q + \frac{1}{C_a} \int q dt = P e^{i\omega t} \quad 2-4$$

where

$q$  = volume flow

$P$  = applied pressure amplitude

The resonant frequency is defined by the condition that  $X_a = \bar{0}$ , resulting in:

$$\omega_0 = c(A_h/l_e V)^{1/2} \quad 2-5$$

The specific acoustic resistance and reactance for a single resonator can be derived from Equations 2-1, 2-2, and 2-3, and are:

$$\theta = a_1 M_n / \sigma \quad 2-6$$

$$\chi = (l_e / \sigma c) \omega - (c A_h / V) \frac{1}{\omega} \quad 2-7$$

where

$\sigma = A_h / A_s$  = the open (neck) to total surface area ratio of the resonator.

The quantities  $a_1$  and  $l_e$  are determined from experimental data. Measurements at higher frequencies (2000 - 6000 Hz) indicate that for perforated plates with hole diameters of about 1 mm a value of  $a_1$  equal to 0.3 results in good agreement between Equation 2-6 and measured data<sup>(5)</sup>. Similarly, experience, as well as data reported in the literature<sup>(6)</sup>, indicates that

$$l_e = 1 + d/2 \text{ (approximately), for zero grazing flow* , and}$$

$$l_e = 1 + d/4 \text{ (approximately), for grazing flows above 30 m/sec* ,}$$

where

$l$  = the physical length of the resonator neck and

$d$  = the diameter of the neck.

A comparison of impedance predicted from this model for a resonator is shown in Figure 2-2. As indicated, good agreement is obtained between predicted and measured reactance for the test conditions. The resistance measurements show more scatter than the reactance measurements. Despite this scatter, there appears to be a decrease in measured resistance with increasing frequency, a result that is at variance with the perforated plate resistance model, Equation 2-6. To retain the concept of a resistance independent of frequency, resistance is taken to be a constant in such a manner that it agrees with the measured data in the vicinity of resonance. In this way, it is expected that peak attenuation, which depends strongly on resistance near the resonant frequency, will be most accurately predicted. The single resonator test results and the validity of the model for single resonators are presented in more detail in Sections 3.1 and 3.3 and, in particular, the error incurred in assuming a resistance independent of frequency is examined.

Two representations of the resistance of uncoupled resonators were used to generate coupled resonator impedance and attenuation predictions. In the coupled resonator optimization studies described below, the resistance of a resonator neck is taken to be independent of frequency and to agree with the measured data in the vicinity of resonance (Figure 2-2). The resistance defined in this way is not in agreement with equation 2-6 for the range of Mach number values and percent open area investigated, but was considered to model the data more accurately. In Figures 3-4 through 3-7 (Section 3.1.2), showing comparisons of predicted and measured impedance of uncoupled resonators, the results of equation 2-6 are indicated for comparison. To improve the resistance model further by taking into account observed dependence of resistance on frequency, a point by point linear curve fit to the measured data was used. The impedance predictions for coupled resonators using this model are compared with measurements in Figures 3-17 through 3-19.

\*Note: Relationships most frequently given in the literature are, for a circular hole,  $l_e = 1 + 0.7d$  without grazing flow and  $l_e = 1 + 0.35d$  with grazing flow greater than 30 m/sec. The accuracy of the expressions given is discussed in Section 3.1.

## 2.1.2 Analytical Modeling of Coupled Resonator Impedance

The three schemes for coupling pairs of resonators that were considered are diagrammed in Figure 2-3. As indicated in the figure, they are referred to as series, parallel, and folded coupling. The essential feature of all three schemes is that an asymmetry is introduced to insure that a pressure imbalance exists across the coupling tube between the two cavities in the frequency range of interest. This causes flow in the coupling tube and energy dissipation in the associated resistive element.

Modeling of the three schemes is accomplished by deriving the equations of motion in terms of the constant parameters described in the preceding section. This leads in each case to a set of equations from which the specific acoustic impedance of the coupled resonator pair can be derived. The values of  $M_i$ ,  $R_i$ , and  $C_i$  are obtained from appropriate measurements in single resonators. Impedance measurements on single resonators with flow are used to determine the parameters  $M_i$  and  $R_i$  for coupled resonator necks with and without flow to determine these parameters for internal coupling tubes. Test results are presented in Section 3.1.

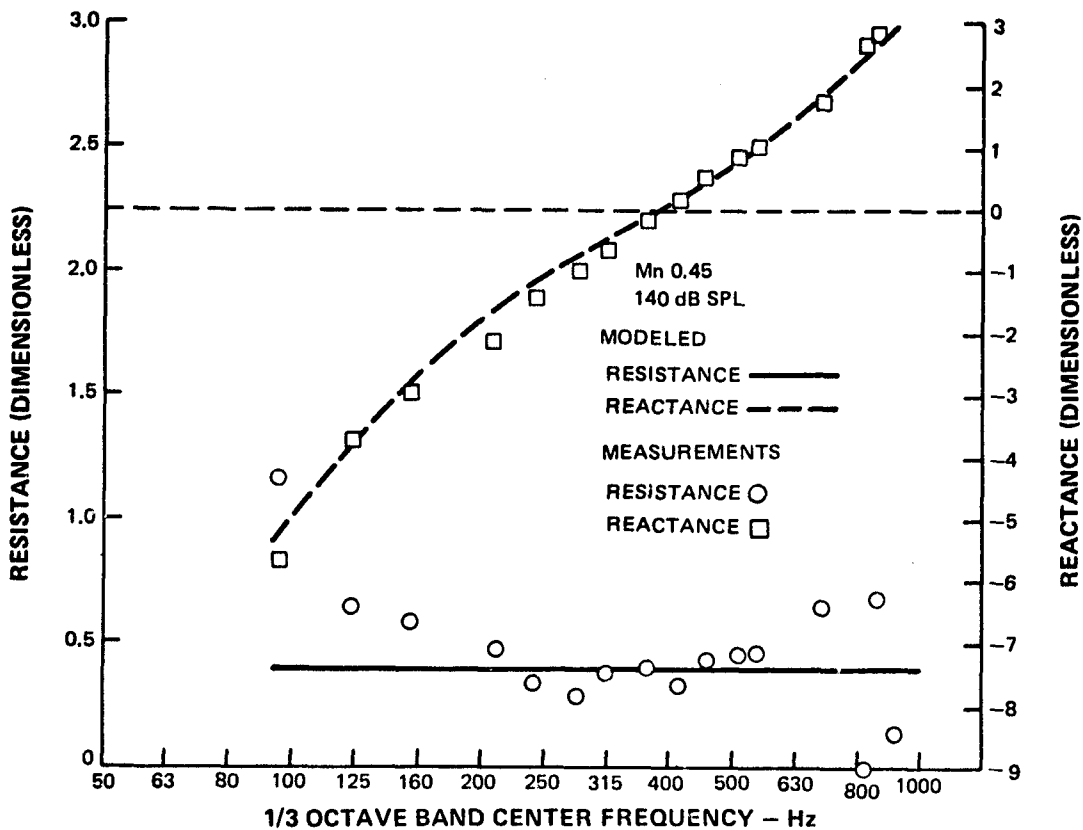


Figure 2-2 Comparison of Single Resonator Impedance Model with Measured Data, Uncoupled Resonator #3 (see Table 3-1)

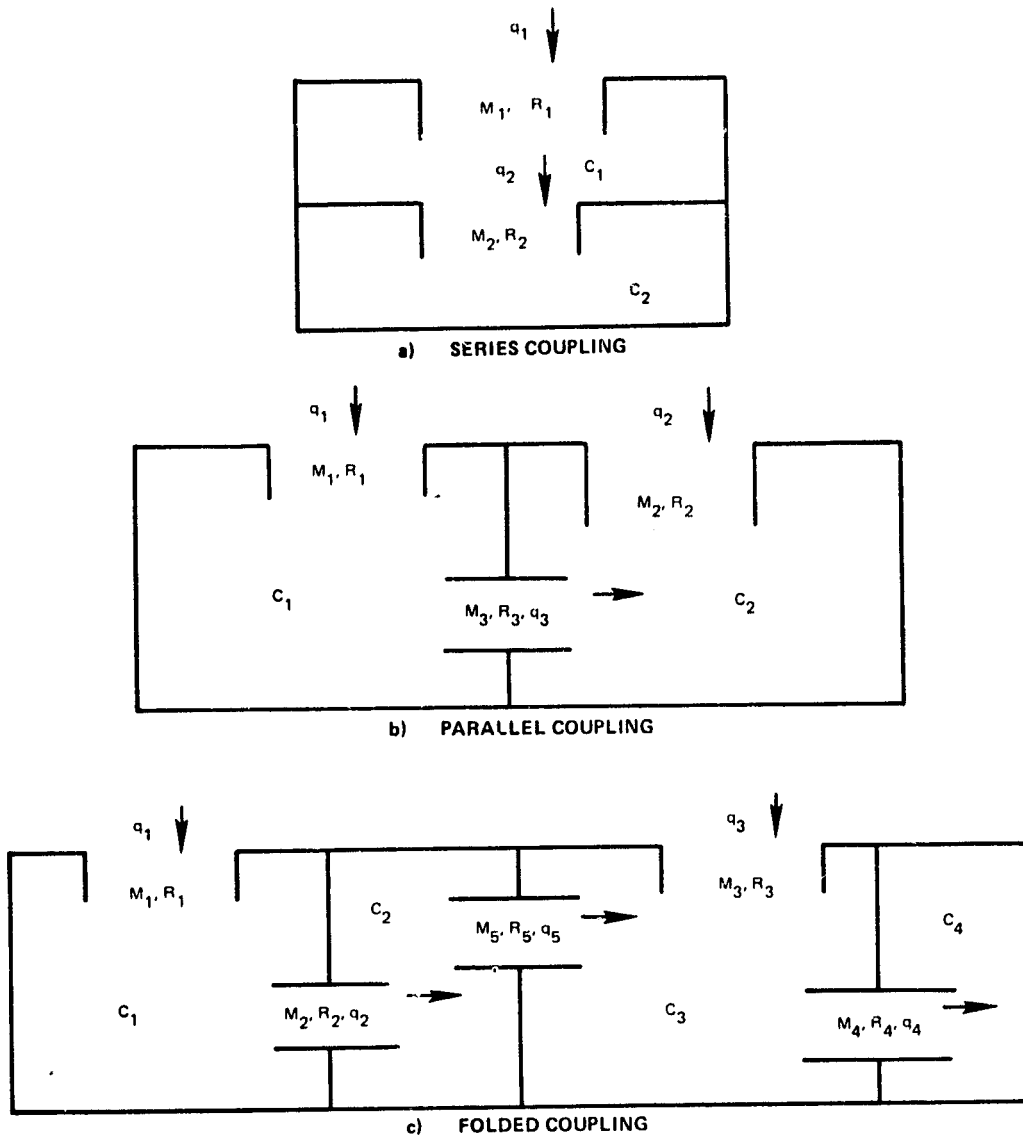


Figure 2-3 Resonator Coupling Schemes

REPRODUCIBILITY OF THE ORIGINAL PAGE IS POOR

### 2.1.2.1 Series Coupled Resonators

The parameters used in modeling the series coupled resonator are indicated in Figure 2-3a. As shown in the figure, there are two mass elements. The equations of motion for the two masses are:

$$M_1 \frac{dq_1}{dt} + R_1 q_1 + \frac{1}{C_1} \int (q_1 - q_2) dt = P e^{i\omega t} \quad 2-8$$

$$M_2 \frac{dq_2}{dt} + R_2 q_2 + \frac{1}{C_2} \int q_2 dt - \frac{1}{C_1} \int (q_1 - q_2) dt = 0 \quad 2-9$$

where M, R, and C are defined in Equations 2-2 and 2-3 above.

These equations relate the acceleration of each mass element (in analogous units) to the sum of the forces on it. In this case, the "spring" restoring force term for  $M_1$  is related to  $(q_1 - q_2)$ , the net flow into volume  $V_1$ , and this same force acts on  $M_2$  in the opposite (positive) sense. The "spring" restoring force on  $M_2$  is related to  $q_2$ , the net flow into  $V_2$ .

Assuming a solution of the form  $q = Q e^{i\omega t}$  and rearranging terms, two equations in two unknowns are obtained:

$$\left( i\omega M_1 + R_1 - \frac{i}{\omega C_1} \right) Q_1 + \left( \frac{i}{\omega C_1} \right) Q_2 = P \quad 2-10$$

$$\left( \frac{i}{\omega C_1} \right) Q_1 + \left( i\omega M_2 + R_2 - \frac{i}{\omega C_1} - \frac{i}{\omega C_2} \right) Q_2 = 0 \quad 2-11$$

These are of the form:

$$a_{11}Q_1 + a_{12}Q_2 = P \quad 2-12$$

$$a_{21}Q_1 + a_{22}Q_2 = 0 \quad 2-13$$

and the solution for  $Q_1$  is:

$$Q_1 = \frac{a_{22}}{a_{11}a_{22} - a_{12}a_{21}} P \quad 2-14$$

The analogous impedance of the system at the point of application of the external pressure is by definition:

$$Z_a = P/Q_1 = \frac{a_{11}a_{22} - a_{12}a_{21}}{a_{22}} \quad 2-15$$

and the specific acoustic impedance, from Equation 2-1, is:

$$\zeta = Z_a A_s / \rho_0 c$$

2-16

A computer program was written to evaluate Equation 2-15 (or 2-16) as a function of frequency. A sample result of this program is presented in Figure 2-4, where  $R_a$  and  $X_a$  are plotted vs. frequency. This result is presented to indicate what was found to be a general feature of coupled resonators. That is, that the rise in reactance with increasing frequency is interrupted because of the coupling, and can even be reversed over a range of frequency. At the same time, a significant increase in resistance occurs. The resistance peak is not in any way related to a non-linear effect associated with a high flow rate through a constriction. The governing equations are strictly linear, and the character of the curves in Figure 2-4 is the result of linear coupling.

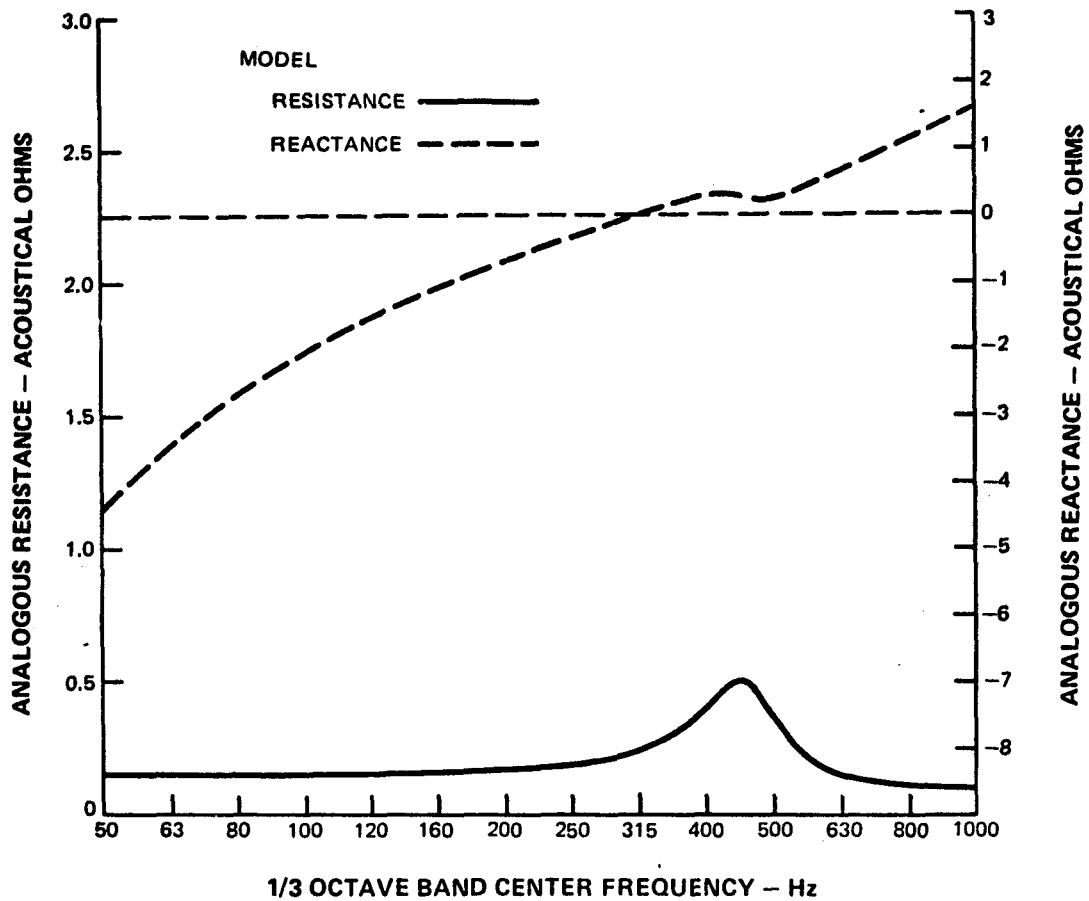


Figure 2-4 Predicted Impedance for a Series Coupled Resonator with  $M_1 = 0.0003 \text{ gm/cm}^4$ ,  $R_1 = 0.10 \text{ gm/cm}^4 \text{ sec}$ ,  $C_1 = 0.00055 \text{ cm}^4 \text{ sec}^2/\text{gm}$ ,  $M_2 = 0.001 \text{ gm/cm}^4$ ,  $R_2 = 1.00 \text{ gm/cm}^4 \text{ sec}$ ,  $C_2 = 0.00015 \text{ cm}^4 \text{ sec}^2/\text{gm}$

### 2.1.2.2 Parallel Coupled Resonators

The approach to modeling parallel coupled resonators is identical to that for series coupling. The parameters for the parallel coupled scheme are defined in Figure 2.3b. As indicated, there are three mass elements identified with the coupling tube and the two necks exposed to flow. The governing equations for the three mass elements are:

$$M_1 \frac{dq_1}{dt} + R_1 q_1 + \frac{1}{C_1} \int (q_1 - q_3) dt = P e^{i\omega t} \quad 2-17$$

$$M_2 \frac{dq_2}{dt} + R_2 q_2 + \frac{1}{C_2} \int (q_2 + q_3) dt = P e^{i\omega t} \quad 2-18$$

$$M_3 \frac{dq_3}{dt} + R_3 q_3 - \frac{1}{C_1} \int (q_1 - q_3) dt + \frac{1}{C_2} \int (q_2 + q_3) dt = 0 \quad 2-19$$

It has been assumed that identical pressures are applied externally at the two resonator neck openings. The assumption is justified by noting that the wavelength is long compared to the distance between the resonator neck openings and the dimensions of the resonators.

Again, assuming a solution of the form  $q = Q e^{i\omega t}$  and rearranging terms:

$$\left( i\omega M_1 + R_1 - \frac{i}{\omega C_1} \right) Q_1 + \left( \frac{i}{\omega C_1} \right) Q_3 = P \quad 2-20$$

$$\left( i\omega M_2 + R_2 - \frac{i}{\omega C_2} \right) Q_2 - \left( \frac{i}{\omega C_2} \right) Q_3 = P \quad 2-21$$

$$\left( \frac{i}{\omega C_1} \right) Q_1 - \left( \frac{i}{\omega C_2} \right) Q_2 + \left( i\omega M_3 + R_3 - \frac{i}{\omega C_1} - \frac{i}{\omega C_2} \right) Q_3 = 0 \quad 2-22$$

These equations must be solved for both  $Q_1$  and  $Q_2$  since the net flow into the coupled resonator system is the sum of these two quantities. The equations above are of the form:

$$a_{11}Q_1 + a_{12}Q_2 + a_{13}Q_3 = P \quad 2-23$$

$$a_{21}Q_1 + a_{22}Q_2 + a_{23}Q_3 = P \quad 2-24$$

$$a_{31}Q_1 + a_{32}Q_2 + a_{33}Q_3 = 0 \quad 2-25$$

and the solutions for  $Q_1$  and  $Q_2$  are obtained in a form similar to Equation 2-14. Finally, the analogous impedance is  $P/(Q_1 + Q_2)$ , the ratio of the applied pressure to the net flow into the coupled resonator. The specific impedance is:

$$\zeta = \frac{P}{(Q_1 + Q_2)} \frac{A_s}{\rho_0 c} \quad 2-26$$

where  $A_s$  is the total surface area of the coupled resonator pair exposed to the driving pressure,  $P$ .

As with the series coupled resonators, the equations for the analogous impedance as a function of frequency were programmed for computer solution, and plots similar to Figure 2-4 were generated for study.

### 2.1.2.3 Folded Coupled Resonators

The parameters of the folded coupled resonator scheme are identified in Figure 2.3c. As indicated in the figure, there are five mass elements, and this leads to five governing equations of motion. The system, as can be seen by comparing Figure 2-3a, b, and c, has the appearance of two series coupled resonators that are in addition coupled in parallel. The equations of motion in the time domain are listed below.

$$M_1 \frac{dq_1}{dt} + R_1 q_1 + \frac{1}{C_1} \int (q_1 - q_2) dt = P e^{i\omega t} \quad 2-27$$

$$M_2 \frac{dq_2}{dt} + R_2 q_2 - \frac{1}{C_1} \int (q_1 - q_2) dt + \frac{1}{C_2} \int (q_2 - q_5) dt = 0 \quad 2-28$$

$$M_3 \frac{dq_3}{dt} + R_3 q_3 - \frac{1}{C_3} \int (q_3 - q_4 + q_5) dt = P e^{i\omega t} \quad 2-29$$

$$M_4 \frac{dq_4}{dt} + R_4 q_4 - \frac{1}{C_3} \int (q_3 - q_4 + q_5) dt + \frac{1}{C_4} \int q_4 dt = 0 \quad 2-30$$

$$M_5 \frac{dq_5}{dt} + R_5 q_5 - \frac{1}{C_2} \int (q_2 - q_5) dt + \frac{1}{C_3} \int (q_3 - q_4 + q_5) dt = 0 \quad 2-31$$

The solution of the equations to define the analogous impedance is rather lengthy. Since it follows exactly the steps described for the series and parallel coupled schemes, it is not given in detail here. Some examples of the computer calculations of the analogous impedance are presented in Section 2.3 along with results for the series and parallel schemes and a discussion of the most promising scheme.

The geometrical parameters of the coupled resonators (i.e., tube lengths and diameters, and cavity volumes) are related to the values of  $M_i$ ,  $R_i$ , and  $C_i$ , determined to be optimum, by models developed from single resonator test results. These models are Equations 2-1 through 2-7 and the test results are presented in Section 3.1.  $M_i$ ,  $R_i$  and  $C_i$  are defined as:

$$M_i = \frac{\rho_o l_{ei}}{A_{hi}}$$

$$C_i = \frac{V_i}{\rho_{oc}^2}$$

$$R_i = a_1 \frac{M \rho_{oc}}{A_{hi}}$$

where

$l_{ei}$  = effective length of the ith neck (cm)

$A_{hi}$  = cross sectional area of the ith neck (cm<sup>2</sup>)

$V_i$  = volume of ith cavity (cm<sup>3</sup>)

### 2.1.3 Analytical Attenuation Calculations

Attenuation predictions for single and coupled resonator panels were made using an existing PWA computer program. This program computes attenuation per centimeter for the first five modes that are functions of the coordinate normal to the treated wall in a rectangular duct of infinite length with one treated wall and an opposing hard wall. The solutions are two dimensional and are functions of the axial coordinate and one cross section coordinate. The input to the program includes wall impedance, duct passage height (distance between the treated wall and opposing hard wall) and free stream Mach number. Attenuation was calculated for the least attenuated mode in terms of pressure wave decay coefficients. The calculation procedure assumes a uniform flow profile in the duct and takes into account an infinitely thin shear layer at the duct walls. This assumption about the shear layer is equivalent to the use of displacement continuity boundary conditions<sup>(8)</sup>. In all cases, including both analytical predictions and test configurations, the duct passage height is 12.7 cm (5 inches) and the length of treatment considered is 50.8 cm (20 inches). Attenuation predictions for the specified length of treatment are taken to be the pressure wave attenuation per centimeter (for an infinitely long duct) multiplied by the treated length.

The program was modified to accept as input either impedance of resonator panels, derived from the analytical models described above, or measured impedance data so that discrepancies between impedance model predictions and test results could be evaluated in terms of differences in attenuation.

## 2.2 LINER OPTIMIZATION

By use of the impedance models and acoustic wave propagation calculations, an attenuation spectrum versus frequency can be predicted for given resonator treatment panel and flow duct conditions. Varying the resonator treatment panel parameters results in changes in the predicted attenuation spectrum, and an optimum can be achieved when the attenuation is maximized in some sense. The optimum impedance at a single frequency is that complex value that gives the maximum attenuation at that frequency and each frequency has a unique value. A liner with an impedance characteristic that follows the optimum in this sense at every frequency over the range of interest would be optimum by any reasonable standard. The properties of such a liner can be defined for purposes of reference, although the construction of such a liner might not be possible in practice. In Figure 2-5, for example, lines of constant attenuation are plotted on a grid of resistance and reactance for a given value of frequency and, as can be seen from the figure, an attenuation maximum of about 0.79 dB/cm exists for this particular case at a specific acoustic impedance of  $\zeta = 0.25 + i 0.24$  at 475 Hz.

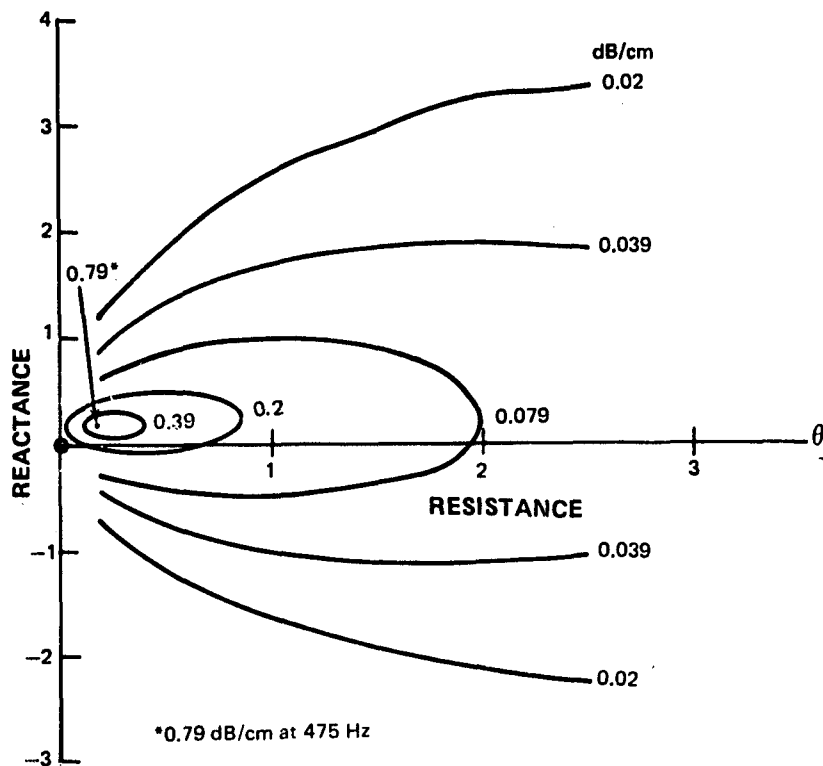


Figure 2-5 Contours of Constant Attenuation in the Impedance Plane,  $M_1=0.45$ , Least Attenuated Mode

The curves of constant attenuation in Figure 2-5 correspond to the duct configuration described in Section 2.1 with a flow Mach number of 0.45\*. By examining similar plots, optima at other frequencies can be defined, and by compiling the results from such plots, the optimum impedance can be charted as a function of frequency. The results of such a study are tabulated in Table 2-1 and plotted in Figure 2-6 along with the impedance of a single resonator. As indicated in the figure, the impedance of a panel of single resonators can intersect the optimum resistance and reactance curves simultaneously at a single frequency, but, as expected from experience, the resonator impedance characteristics are such that they tend to be near the optimum over only small range of frequencies.

\*NOTE: This corresponds to the baseline uncoupled resonator conditions and the conditions for which the coupled resonators are to be optimized. See Section 2.4.

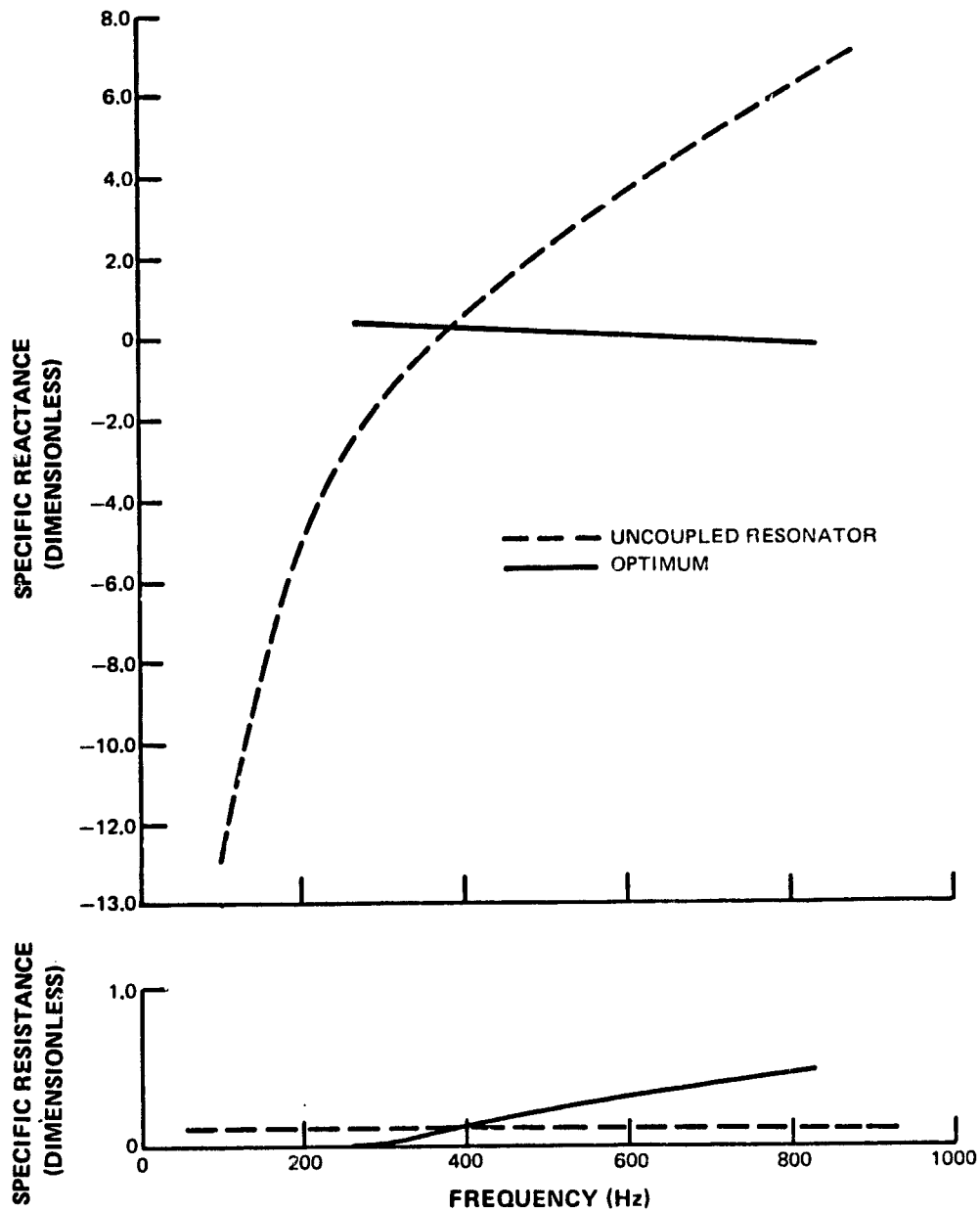


Figure 2-6 Optimum Resistance and Reactance for Sample Uncoupled Resonator,  $Mn = 0.45$

Given a liner with an infinite number of adjustable parameters, or degrees of freedom, the boundary impedance of the duct could, in theory, be adjusted to match the optimum over a wide range of frequencies, and the attenuation as a function of frequency would match the values in Table 2-I.

TABLE 2-1

**OPTIMUM RESISTANCE AND REACTANCE  
FOR TYPICAL MACH NUMBERS AND FREQUENCIES**

Mach No.	Frequency Hz	Resistance (Dimensionless)	Reactance (Dimensionless)	Attenuation (dB/cm)
0	200	0.12	-0.11	9.2
0	360	0.20	-0.22	8.4
0	640	0.40	-0.40	7.2
0.27	220	0.05	0.21	7.3
0.27	440	0.25	0.10	6.9
0.27	770	0.48	-0.12	4.9
0.45	230	0.01	0.42	5.6
0.45	480	0.25	0.24	4.2
0.45	830	0.48	-0.04	3.4

### 2.2.1 Optimization Criteria For Uncoupled and Coupled Resonators

In the absence of enough adjustable parameters to optimize attenuation at every frequency over the desired range, it becomes necessary to redefine the optimization problem. If, for example, the spectrum of noise to be attenuated is a pure tone, the optimum liner is the one that gives maximum attenuation, as described in the preceding section, at the frequency of the tone. Clearly, a panel of uncoupled resonators capable of meeting the optimum criterion of the preceding section would be entirely suited to this spectrum. If the energy in the spectrum is spread continuously over a range of frequency, however, the optimum liner may consist of resonators damped to give a modest attenuation over the range without being optimum in the sense of the previous section at any frequency. To define the optimization problem, it is necessary to specify both the spectrum of noise to be attenuated and the property of the spectrum to be minimized.

The spectrum used to define an optimization criterion for the various coupled and uncoupled resonant liners investigated under this program is a typical low frequency core engine noise spectrum presented in Figure 2-7. As indicated, the spectrum peaks at 400 Hz. The property of the spectrum to be minimized is the perceived noise level (PNL) with the length of treatment held constant (50.8 cm). Treatment width (50.8 cm) and depth (10.2 cm) are also held constant, and all dimensions are the same as used for the P&WA uncoupled baseline panel (see Section 2.4). With these constraints, the optimization problem is defined, and this criterion is used in dealing with evaluation and optimization of single and coupled resonator liners.

### 2.2.2 Alternate Optimization Criterion

As a practical matter, the decrease in PNL may be specified, for example, for a turbofan engine to meet a specified noise requirement. In this case it may be desired to minimize the length of treatment required by varying the liner parameters with the PNL reduction held

constant. In Section 3.4, in which the coupled resonator concept is evaluated in comparison to the optimum single resonator design, this criterion as well as the one of the previous section is applied as a measure of effectiveness.

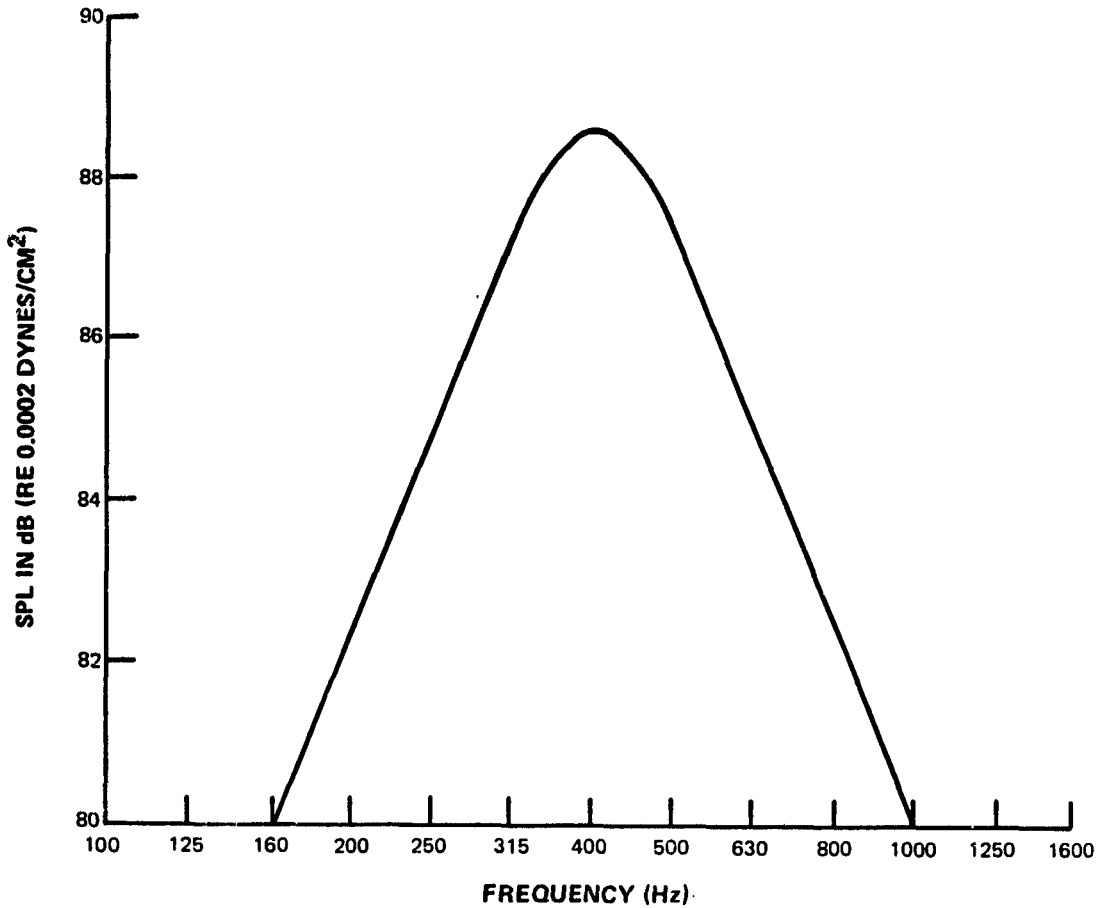


Figure 2-7 Low Frequency Core Noise Spectrum

### 2.3 SELECTION OF COUPLED RESONATOR CONFIGURATIONS FOR TEST

The three coupled resonator geometrical configurations were evaluated relative to each other by generating a series of predicted attenuation versus frequency curves and seeking those designs that provided significant attenuation over an octave band centered near 400 Hz. The annoyance (noy) values of the attenuated source spectrum of Figure 2-7 were then examined for those designs to determine the most promising coupling scheme. Finally, the parameters of the governing equations for the most promising scheme were varied to minimize the PNL with regard to the source spectrum.

In all cases, attenuation predictions were generated for a duct treated on one side with 50.8 cm (20 inches) of treatment, a spacing of 12.7 cm (5 inches) between treatment and the opposing hardwall, and a duct flow Mach number of 0.45. These conditions of duct flow and geometry correspond to the conditions under which the uncoupled resonator panel baseline data were generated and are representative of the Mach numbers and geometry in an engine tailpipe, where core noise absorption would be placed.

### 2.3.1 Series Coupled Resonator

The series coupled resonator, Figure 2-3a, is the least complex of the coupled resonator configurations. The six parameters that can be varied are identified in the figure.

The total enclosed volume is fixed by the criteria established in Section 2.2, reducing the number of variables to five. Furthermore, curves of analogous resistance versus frequency indicate that the coupled resonator resistance is always equal to or larger than the resistance associated with the hole exposed to flow. To keep the system resistance low,  $R_1$  was set equal to 0.1 (dimensionless). This represented the smallest practical value that could be achieved with a grazing flow of Mach number 0.45. Data to support this value are presented in Section 3.1. The choice of  $R_1$  reduces the number of variables to four.

For the series coupled resonator, the relationship between parameters in analogous and dimensionless units (see Equations 2-1 through 2-7) is:

$$\zeta = \frac{A_s}{\rho_0 c} \quad Z = \frac{103}{41.6} \quad Z = 2.47 Z \quad 2-32$$

A list of typical values of the four variables and the predicted attenuations are given in Table 2-II. The highest attenuation predicted for all frequencies over the 400 Hz octave band, as indicated in the table, was found to be 0.083 dB/cm. The design that yielded this result was selected to be the "best" of the series coupled designs, and was compared to similarly selected designs for the parallel and folded coupled designs.

TABLE 2-II

ATTENUATION OF VARIOUS SERIES COUPLED CONFIGURATIONS

All parameters in analogous cgs units

CONSTANTS:

$$R_1 = 0.1$$

$$C_1 + C_2 = 0.0007$$

Variable Parameters

$M_1$	$C_1$	$R_2$	$M_2$	Attn dB/cm
0.0002	0.00055	1.0	0.0007	0.067
0.00025	0.00055	1.0	0.0007	0.083*
0.0003	0.00055	0.9	0.0008	0.079
0.0003	0.00055	1.0	0.0008	0.079
0.0003	0.00055	1.5	0.001	0.079
0.0003	0.00050	1.5	0.001	0.071
0.0003	0.00065	1.5	0.001	0.043

\* "best" configuration

2.3.2 Parallel Coupled Resonator

The parallel coupled resonator, Figure 2.3b, is a more complex coupled configuration. It requires definition of resistance and mass for three tubes and capacitance for the two volumes, giving eight parameters in all. As with the series resonator described above, the total volume remains constant and the resistance of the tubes open to the duct should be small. The discussion of the previous section continues to be valid, and in this case, three of the parameters are fixed. This leaves five parameters to be varied.

The values of the five parameters that were varied and the measure of attenuation achieved over an octave band centered at 400 Hz, are presented in Table 2-III. The parameter values leading to the highest attenuation as determined by this criterion are indicated in the table. By comparing attenuation values from Tables 2-II and 2-III, the highest attenuation achieved over an octave band centered near 400 can be seen to be 0.10 dB/cm for the parallel coupled design. This represents a 20 percent improvement over the best series coupled resonator configuration.

TABLE 2-III

ATTENUATION OF VARIOUS PARALLEL COUPLED CONFIGURATIONS

All parameters in analogous cgs units      CONSTANTS:       $R_1 = R_2 = 0.1$   
 $C_1 + C_2 = 0.0014$

Variable Parameters					Attn. dB/cm
$M_1$	$C_1$	$M_2$	$R_3$	$M_3$	
0.0001	0.0006	0.0004	2.0	0.0004	0.083
0.00015	0.0006	0.0004	2.0	0.0006	0.10*
0.00015	0.0006	0.0004	1.5	0.0006	0.098
0.00015	0.0006	0.0004	3.0	0.0006	0.098
0.0002	0.0008	0.0008	1.0	0.0008	0.079
0.0002	0.0008	0.0009	1.0	0.0005	0.071
0.00025	0.0007	0.0008	1.0	0.0004	0.059

\* "best" configuration

**2.3.3 Folded Coupled Resonator**

The folded resonator configuration, Figure 2-3c, is the most complex of the three coupled resonator configurations. In all, as shown in Figure 2-3c, there are five coupling tubes for which mass and resistance must be defined and four volumes for which capacitance must be defined for a total of fourteen parameters. Fixing the total volume and the resistance of the tubes exposed to flow, as discussed in the previous sections, reduces the number of parameters to be varied to eleven.

In order to have an organized approach to the problem of optimizing this configuration, the folded coupled resonator is considered as two series resonators coupled in parallel. The parameters of the two series resonators are chosen to correspond to the optimum for a series coupled resonator, and the coupling tube parameters,  $R_3$  and  $M_3$  in Figure 2-3c, are adjusted until an optimum design is achieved. This results in a restrictive optimization of the folded coupled configuration. However, no variation of the parameters, including those listed as constant in Table 2-IV for this configuration, was found that led to a better result than the

“best” of Table 2-IV. The folded coupled configuration has one and a half times as many design parameters as the parallel coupled configuration, and in the sense of the discussion in Section 3.4, should have a greater potential for optimization over a range of frequency. This potential, if it exists for the folded coupled configuration, was not realized during the course of the study.

Some values of the parameters assumed and the resulting 400 Hz octave band attenuations are presented in Table 2-IV. As indicated in the table, the maximum attenuation over an octave is 0.098 dB per cm and on this basis the folded coupled configuration is predicted to be about as good as the parallel coupled configuration.

TABLE 2-IV

ATTENUATION OF VARIOUS FOLDED COUPLED CONFIGURATIONS

All parameters in analogous cgs units		CONSTANTS:	
$R_1 = 0.1$		$M_1 = 0.0003$	$C_1 = 0.0005$
$R_2 = 1.0$		$M_2 = 0.001$	$C_2 = 0.0002$
$R_4 = 0.1$		$M_4 = 0.0003$	$C_3 = 0.0005$
$R_5 = 1.0$		$M_5 = 0.001$	$C_4 = 0.0002$
$R_3$		$M_3$	Attenuation dB/cm
1.5		0.0006	0.043
2.0		0.0006	0.047
1.0		0.001	0.059
2.0		0.0015	0.091
2.0		0.002	0.098*

\* “best” configuration

2.3.4 Selection of the Most Promising Scheme

By comparing the predicted attenuations for the three coupling schemes, the parallel coupling scheme is predicted to be more effective than the series coupling scheme. The folded coupling scheme, however, is about as effective as the parallel. To aid in further evaluating the three

coupling schemes, the 1/3 octave band noy values for the source spectrum, as attenuated by the best series, parallel, and folded coupled resonator designs (from Tables 2-II, III, and IV) were determined, and the results are plotted in Figure 2-8. Also shown in the figure are the corresponding noise levels of the attenuated source spectrum in PNdB. These PNdB values should not be taken as the lowest that can be achieved with any of the configurations since they have not been optimized at this point with respect to minimizing the perceived noise level. As indicated, the parallel coupled configuration is again shown to be as good as or better than the other two coupling schemes.

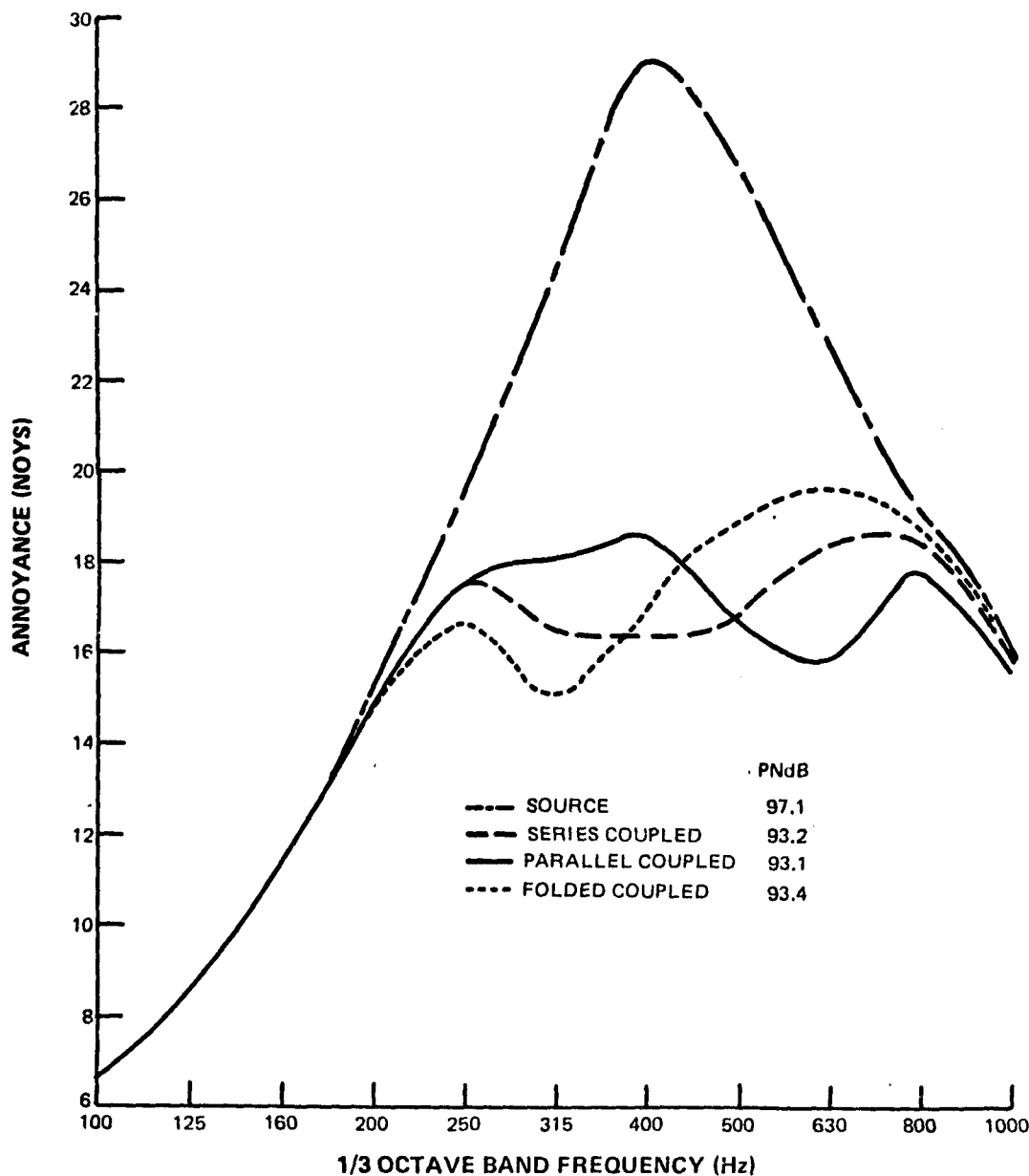


Figure 2-8 Comparison on an Annoyance Basis of Predicted Performance of the Three Coupling Schemes

Because of these considerations, and because the folded coupling scheme is relatively complex, the parallel coupling scheme was chosen for optimization according to the criteria of Section 2.2 and for fabrication and test. This choice resulted in a configuration for test that could be constructed with a maximum assurance that the resonator parameters were in fact close to the design values.

### **2.3.5 Definition of the Optimum Parallel Coupled Resonator Configuration**

The best values of the parallel coupled resonator parameters were taken as a starting point to optimize this coupling scheme according to the criterion of Section 2.2. The various parameters, with the exception of the total resonator volume but including the resistances of the tubes open to flow, were varied holding the treatment length constant at 50.8 cm. until the PNL of the source spectrum was minimized. The parametric variation was performed by using the models described in Section 2.1 of this report.

A partial list of the parameter values considered and the predicted PNL of the attenuated source spectrum for each configuration are presented in Table 2-V. As indicated in the table, the predicted PNL is more sensitive near optimum to changes in the parameters of the tubes exposed to flow than to be parameters of the coupling tube.

The parameter values listed in Table 2-V are in the analogous units described in Section 2.1, and the next step was to translate these to hardware design variables, such as tube length, diameter, etc., so that models could be fabricated for impedance and attenuation tests. Analogous units were convenient to use during this phase of the study. The conversion to dimensionless units is given in Equation 2-32.

To accomplish this, the models of Section 2.1 were used to relate the M, R, and C parameters to geometrical lengths. Single resonator test results, described in detail in a later section, were used to relate grazing flow controlled resistance to resonator neck geometry and to determine effective length with and without flow. The equations of Section 2.1, were used to calculate the impedance of the optimum coupled resonator.

The resulting resonator dimensions are listed in Table 2-VI along with the dimensions of the optimum. As can be inferred from the table and Figure 2-9, all designs can be constructed without violating physical constraints.

TABLE 2-V

OPTIMUM PARAMETERS FOR PARALLEL  
COUPLED CONFIGURATIONS

CONSTANTS:  $C_1 = C_2 = 0.0014$

$R_1$	$R_2$	$R_3$	$M_1$	$M_2$	$M_3$	$N^*$
0.25	0.25	1.5	0.0002	0.0004	0.0005	31.9**
0.15	0.25	1.5	0.0002	0.0004	0.0005	32.2
0.25	0.25	2	0.0002	0.0004	0.0005	31.9**
0.25	0.25	1.0	0.0002	0.0004	0.0005	32.6
0.25	0.25	1.5	0.0015	0.0004	0.0006	32.0
0.25	0.25	1.5	0.0025	0.0005	0.0006	34.0
0.25	0.25	1.5	0.0002	0.0005	0.0006	32.5
0.25	0.25	1.5	0.0002	0.0035	0.0006	32.6

\*N = annoyance of treated source spectrum

\*\*optimum configurations

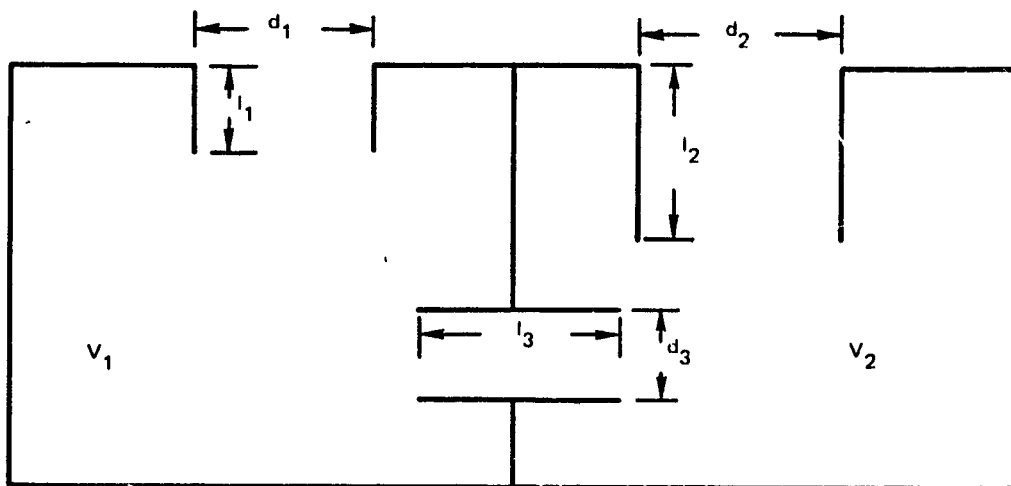


Figure 2-9 Parallel Coupled Resonator Geometric Parameters

**TABLE 2-VI**  
**SUMMARY OF COUPLED RESONATOR**  
**DESIGN PARAMETERS**

Parameter	Optimum	Off-Optimum	
		A	B
$d_1$ , cm	5.9	6.2	5.0
$l_1$ , cm	1.5	1.9	1.1
$l_{1e}$ , cm	3.0	3.4	2.3
$d_2$ , cm	5.9	6.2	5.0
$l_2$ , cm	6.5	7.5	5.4
$l_{2e}$ , cm	8.0	9.0	6.6
$d_3$ cm	4.1	4.1	4.1
$l_3$ cm	1.9	1.9	1.9
$l_{3e}$ cm	3.9	3.9	3.9
$V_1$ cm <sup>3</sup>	1000	1000	1000
$V_2$ cm <sup>3</sup>	1000	1000	1000
$R_3$ RAYLS	26	26	26

### 2.3.6 Definition of Two Off-Optimum Parallel Coupled Resonator Configurations

Relating the desired resistance of the resonator necks, when exposed to grazing flow, to physical dimensions was considered to be the least accurate procedure in defining the optimum resonator. In addition, the predicted sensitivity of the optimum design to the values of these resistances resulted in the choice of the neck resistance as the parameter to vary to arrive at off-optimum designs for test. Correspondingly, the two off-optimum configurations were designed to have a predicted 20 percent increase and decrease in resistance, relative to the optimum.

## 2.4 ANALYTICAL EVALUATION OF COUPLED RESONATORS

In this section, analytical predictions of attenuation spectra and source spectrum PNL reduction are presented. Comparisons are made between the predictions for the P&WA baseline

uncoupled resonator panel, an “improved” uncoupled resonator baseline panel, and the three coupled resonator configurations discussed in Section 2.3. The duct geometry and treatment length are held constant as described in Section 2.1, and the duct flow Mach number is kept constant at a value of 0.45. The impedance variation with frequency is predicted by the use of the models described in Section 2.1. The attenuation spectrum is predicted by use of the method described in Section 2.1.3.

#### 2.4.1 Baseline and Improved Baseline Attenuation Predictions

The P&WA uncoupled resonator baseline data were obtained from a panel of resonators such as shown in Figure 2-10. The enclosed volume had been fixed at  $1000 \text{ cm}^3$  and the neck open area at  $10 \text{ cm}^2$  (10% of the surface area), resulting in a configuration whose dimensions were small compared to wavelengths in the core engine spectrum frequency range. The requirement that peak attenuation occur at 400 Hz fixed the mass parameter,  $M$ , associated with the resonator neck. Subsequently an analytical study was made to optimize the resonator configuration in the sense discussed in Section 2.2.1 by varying the neck open area (i.e., the resistance parameter) while holding the volume constant.

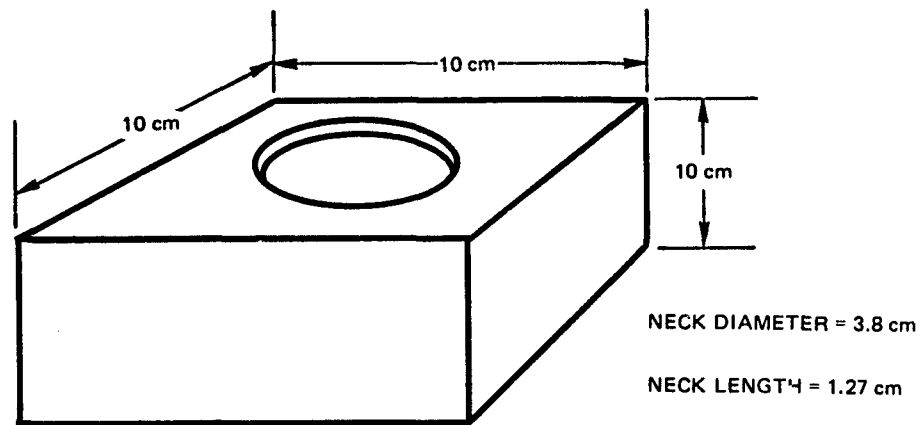


Figure 2-10 P&WA Baseline Resonator

The result of this study was an improved baseline resonator design, and although this configuration was never built and tested it was retained as the optimum uncoupled configuration and was used as a basis of comparison for analytical evaluation of the coupled resonator concept.

The values of the analogous parameters of the baseline, predicted from Equations 2-1 through 2-7, and the improved baseline are presented in Table 2-VII along with the predicted source spectrum PNL reduction achieved by the two configurations. As indicated in the table, the P&WA baseline resonator is predicted to have a somewhat higher than optimum neck resistance.

TABLE 2-VII

BASELINE RESONATOR PARAMETERS,  $M_n = 0.45$ 

	P&WA Baseline	Improved Baseline
Ra	0.478	0.312
Ma	0.000236	0.000236
Ca	0.00077	0.00077
$\Delta$ PNL predicted	2.8	3.8

#### 2.4.2 Optimum and Off-Optimum Coupled Resonator Panel Predicted Attenuation

Predicted attenuation for panels of the optimum and two off-optimum coupled configurations are presented in Figure 2-11. The off-optimum A configuration is shown in the figure to have a higher peak attenuation than the optimum. However, when plotted in terms of annoyance units, Figure 2-12, it can be seen that the attenuation provided by the optimum configuration between 315 and 630 Hz results in a more balanced curve with the optimum giving the lowest perceived noise level.

#### 2.4.3 Analytical Evaluation of the Coupled Resonator Concept

A comparison of the predicted attenuation spectra of the P&WA baseline, improved baseline, and optimum parallel coupled resonator configurations are presented in Figure 2-13. As can be seen, the coupling scheme, when compared to results for uncoupled resonators, is predicted to result not only in an increase in peak attenuation of about 50 percent but also in bandwidth of about 1/3 octave. It should be emphasized that the higher peak attenuation for the coupled resonator configuration is calculated under the constraint of minimizing the PNL of the attenuated source spectrum. Both the coupled and uncoupled configurations are capable of the same peak attenuation with this constraint removed, although the uncoupled resonators would exhibit a reduced bandwidth of attenuation.

These results applied to the source spectrum and transformed to annoyance units are plotted in Figure 2-14. The figure indicates in a general way the manner in which the increased attenuation and bandwidth of the coupled scheme results in a reduction in PNL over that obtained with the uncoupled resonators. The calculated PNL reduction of the source spectrum achieved by the P&WA baseline, improved baseline, and three coupled configurations are tabulated in Table 2-VIII. All coupled configurations show about the same PNL reduction and the optimum shows a 90 percent improvement over the P&WA baseline and a 40 percent improvement over the improved baseline.

REPRODUCIBILITY OF THE ORIGINAL PAGE IS POOR

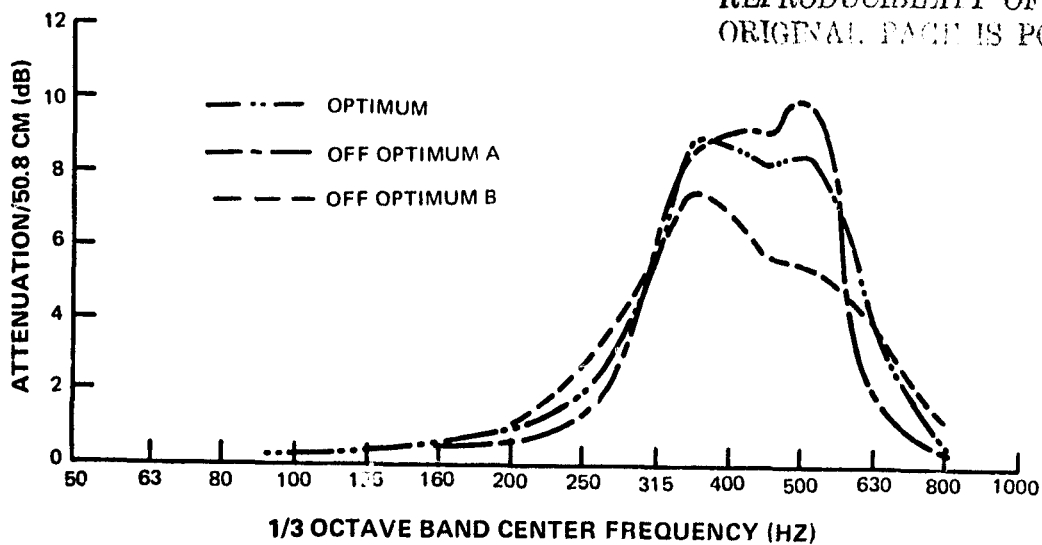


Figure 2-11 Comparison of Predicted Coupled Resonator Attenuation,  $MN = 0.45$

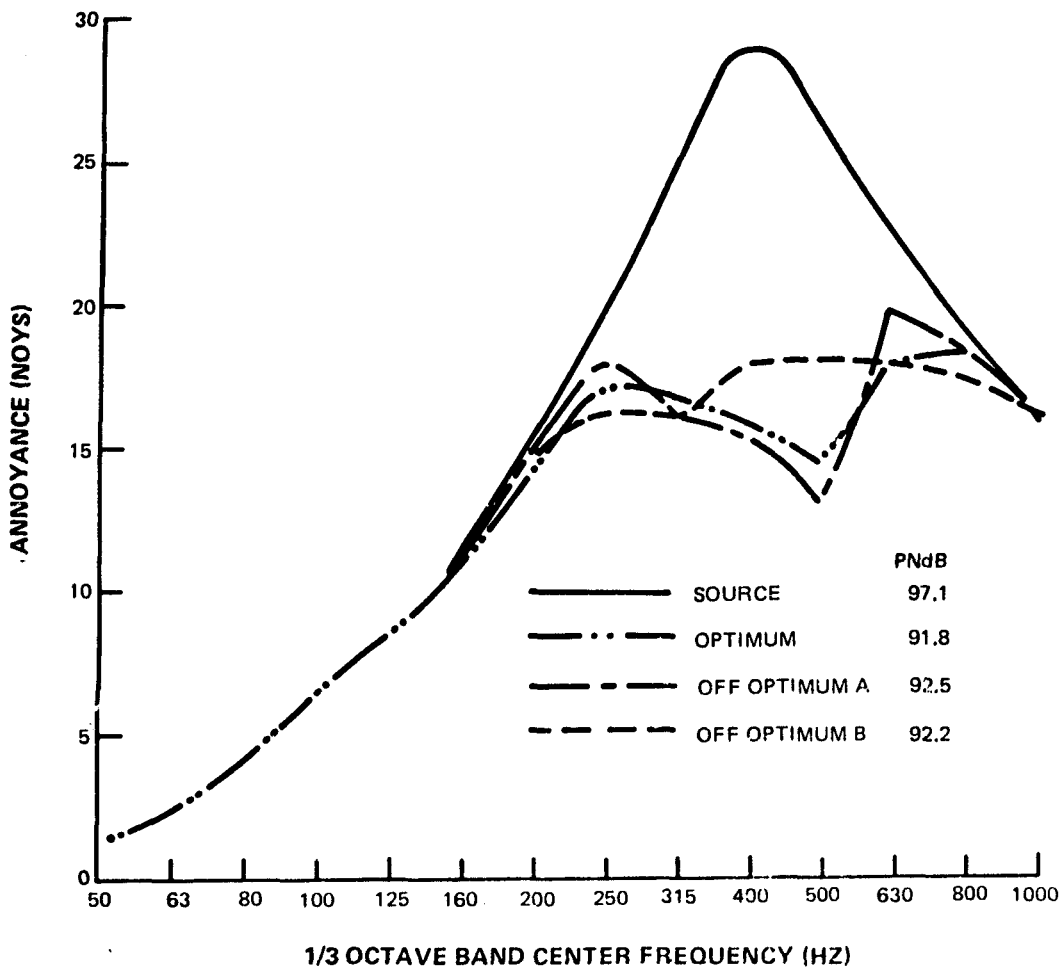


Figure 2-12 Comparison of Predicted Effects of Coupled Resonators on Source Spectrum in Annoyance Units,  $Mn = 0.45$

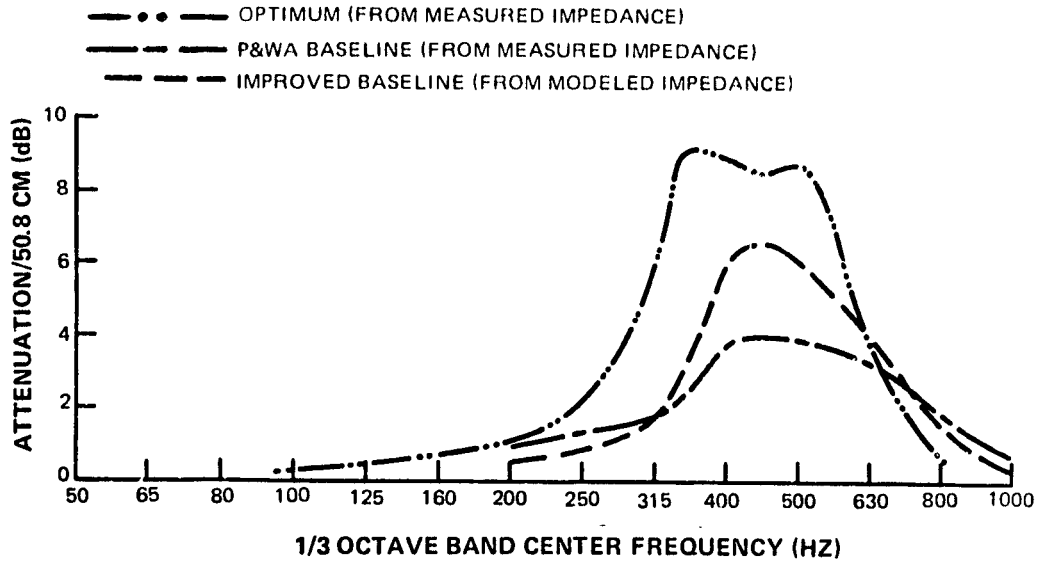


Figure 2-13 Comparison of Predicted Attenuation for Coupled and Uncoupled Baseline Resonators,  $M_n=0.45$

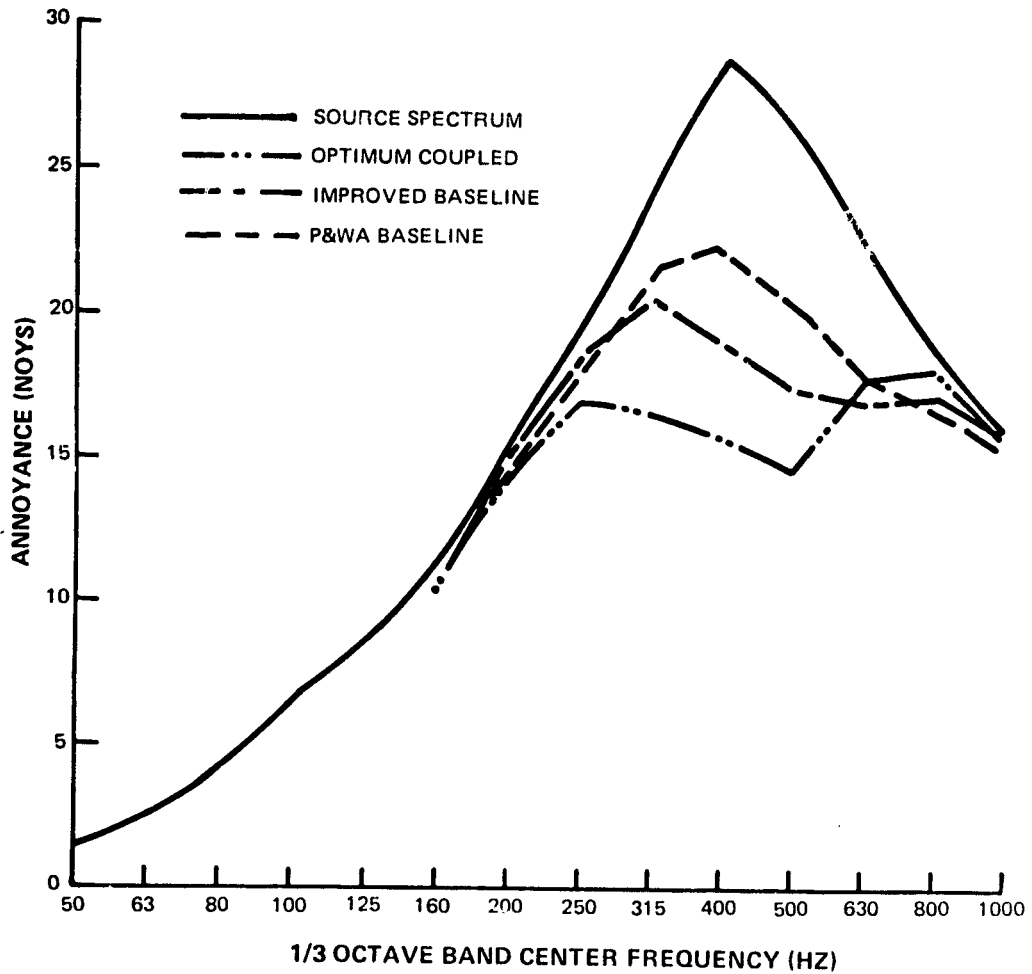


Figure 2-14 Comparison of Predicted Effects of Coupled and Uncoupled Baseline Resonators on Source Spectrum in Annoyance Units,  $M_n=0.45$

Impedance and attenuation measurements were performed on the optimum and two off-optimum designs to provide confirmation of the analytical models and guidance for the improvement of the model. These test results and resulting comparisons are described in Section 3.1.

Table 2-VIII

PREDICTED PNL REDUCTION OF SOURCE SPECTRUM ACHIEVED  
BY 50.8 CM OF BASELINE AND COUPLED RESONATORS,  $M_n = 0.45$

Configuration	Noys	PNL	$\Delta$ PNL
Source	52.3	97.1	— —
Off-Optimum A	38.1	92.5	4.6
Optimum	36.4	91.8	5.3
Off-Optimum B	37.2	92.2	4.9
Baseline	43.0	94.3	2.8
"Improved" Baseline	40.3	93.3	3.8

### 3.0 TEST PROGRAM

#### 3.1 RESONATOR IMPEDANCE TESTS

Impedance measurements were performed both on uncoupled and coupled resonators to verify analytical predictions developed in Section 2.0. Specifically, the testing was directed toward checking the equations for modeling the resonator parameters in terms of geometry (Equations 2-1 through 2-7) and the impedance predictions derived from the governing equations of the parallel coupled resonators (Section 2.1).

In the following sections, the test facility and impedance measurement instrumentation is described, and the equations for deriving impedance from the raw pressure and phase data are derived. Finally, typical examples of comparisons of model results with measured data are presented.

##### 3.1.1 Impedance Test Facility

The test specimen was mounted on one wall of the flow duct facility shown in Figure 3-1. The figure includes a close-up view of the location of the test specimen. A high amplitude driver was used to excite the upstream chamber to provide the required (approximately) sinusoidal sound pressure level at the surface of the test piece.

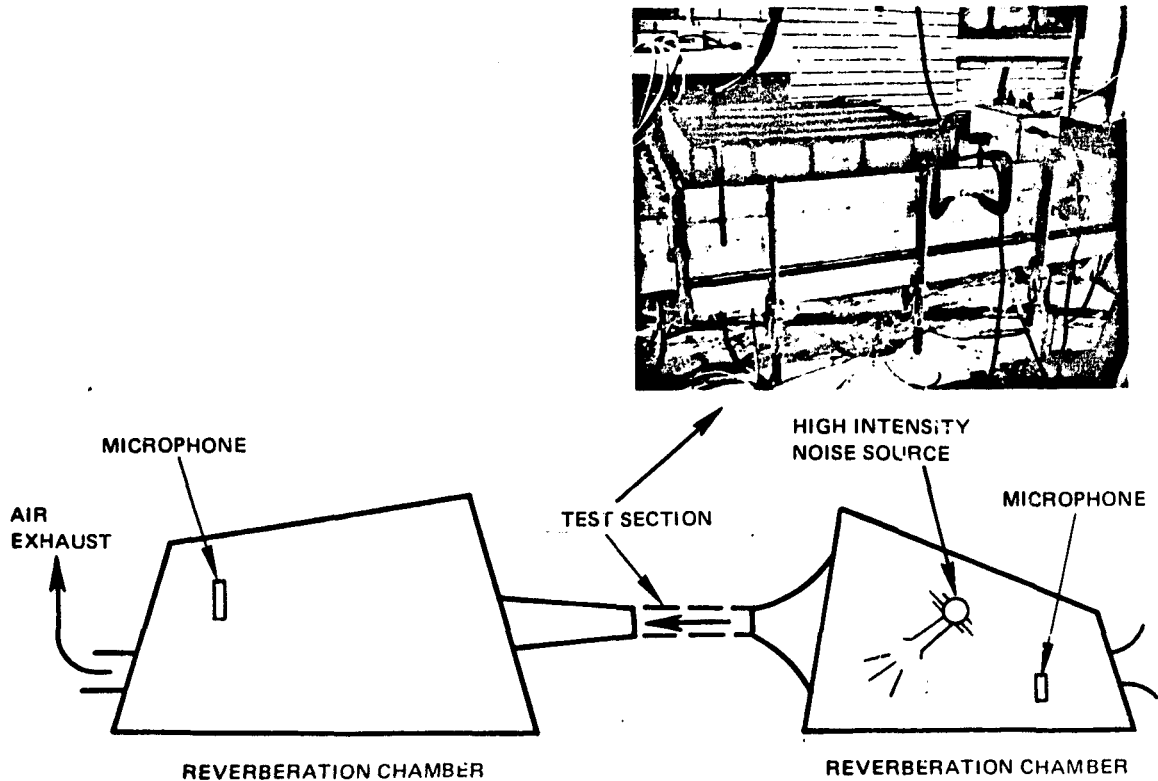


Figure 3-1 Flow Duct Facility

The system for taking data is diagrammed in Figure 3-2. As shown in the figure, the same oscillator used to excite the acoustic driver is used to tune tracking filters. From the outputs of the filters, phase and amplitude measurements of pairs of microphone signals were made. Amplitudes were measured using a true RMS voltmeter with a time constant adjustable as required to average statistical fluctuations that occur with flow. The relative phase of the two signals was measured on line using a portable cross correlation computer. The flow duct facility is capable of providing grazing flow over the test specimen in excess of Mach number 0.45. The cross correlation function of two filtered microphone signals is a cosine function displaced from the zero delay time axis by a phase angle equal to the phase difference between signals. Because of the averaging performed by the correlator, this system was found to be relatively immune to fluctuations occurring with flow as compared to an available phase meter.

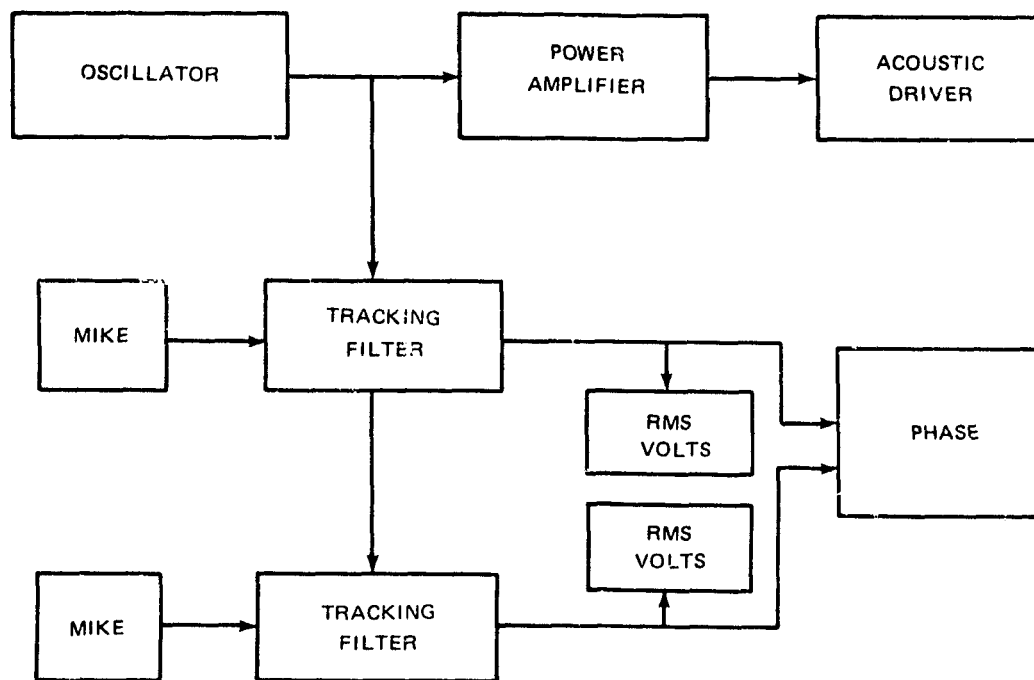


Figure 3-2 Impedance Data System

Placement of the two microphones for uncoupled resonator impedance measurements is shown in Figure 3-3. In the frequency range of interest, the most satisfactory location for the duct microphone was on the duct wall opposite the specimen. The other microphone was located in the resonator cavity.

At low frequencies, the pressure in the cavity is related to the time integral of the volume flow through the resonator neck. The cavity microphone, therefore, measures the volume velocity in the cavity neck, and the duct microphone measures the driving pressure. The relationship between cavity pressure and volume velocity is:

$$p_2 = P_2 e^{i\omega t} e^{i\phi} = \frac{1}{Ca} \int q dt = - \frac{iq}{\omega Ca}$$

3-1

from which the impedance can be calculated by the equations:

$$p_1 = P_1 e^{i\omega t} \quad 3-2$$

$$Z_a = P_1/q = - \frac{i P_1}{\omega C_a P_2 e^{i\phi}} \quad 3-3$$

where

$P_1$  = the duct pressure

$P_2$  = the cavity pressure

$q$  = volume velocity in the resonator neck

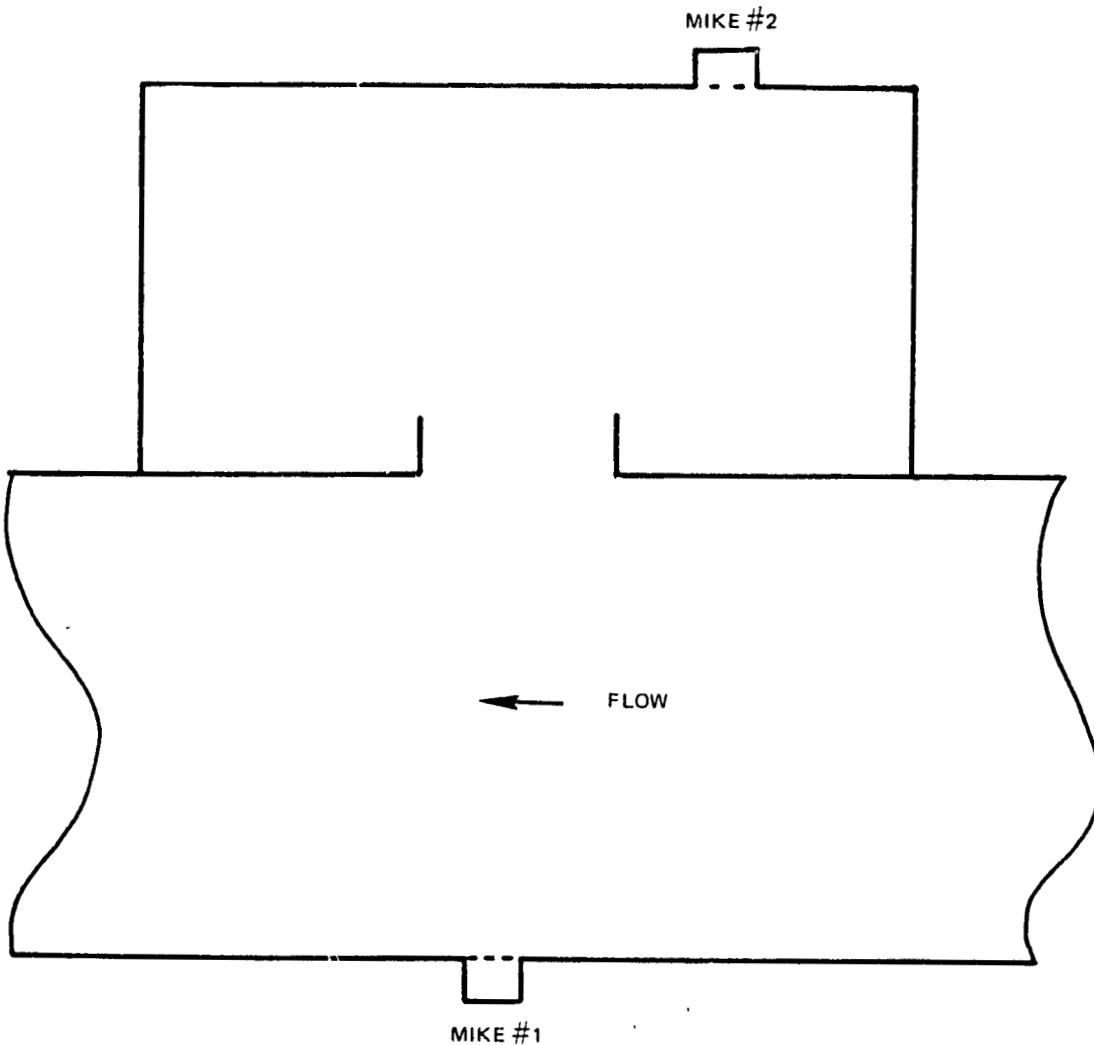


Figure 3-3 Microphone Placement for Uncoupled Resonator Impedance Measurements

The test matrix consisted of impedance measurements of three single resonators at 0, 0.27, and 0.45 grazing flow Mach number and at 130dB and 140dB sound pressure level at the duct microphone. The physical characteristics of the three resonators are listed in Table 3-1. As indicated in the table, the three resonators were chosen to cover a 10 to 30 percent open area range. The lowest percent open area is the same as was used for the P&WA baseline resonators, and 30 percent is the highest used in defining the coupled resonators for test.

TABLE 3-1

UNCOUPLED RESONATOR GEOMETRICAL PARAMETER VALUES

Parameter	Resonator		
	No. 1	No. 2	No. 3
d, cm	3.18	4.80	5.72
l, cm	1.02	3.13	5.47
V*, cm <sup>3</sup>	785.4	785.4	785.4
σ, %	9.8	22.3	31.6

\*Note: Cavities are 10 cm diameter cylinders, 10 cm deep

**3.1.2 Uncoupled Resonator Measured Impedance & Comparisons With Predicted Values**

The data from these tests were used to calculate the impedance of panels of uncoupled resonators. By comparing the measured and predicted results, the validity of the models described in Section 2.1 was determined and the required experimentally derived constants assigned.

**3.1.2.1 Effect of Resonator Geometry**

A comparison of the single resonator parameter models in specific (dimensionless) acoustic units (Equations 2-6 and 2-7) with measured data from the three uncoupled resonators at the design duct flow Mach number, 0.45, is presented in Figures 3-4, 3-5 and 3-6. As indicated in the figures, the predicted and measured reactances are in good agreement. Since the predicted reactance curves are dominated by the analogous spring parameter,  $C_a$ , at frequencies well below resonance, and the analogous mass parameters,  $M_a$  becomes important somewhat below resonance, agreement in both frequency ranges indicates that both parameters have been modeled correctly in terms of the resonator geometry and duct flow. The effective length used for the resonator neck was the actual length, l, plus 1/4 the diameter, d, (rather than  $l + 0.35d$ ) as discussed in Section 2.1. This formula gave better agreement between predictions and measurements at both 0.27 and 0.45 Mach number flows.

As can be seen in Figures 3-4, 3-5 and 3-6, the measured resistance tends to decrease with increasing frequency. In addition, the values of resistance as calculated using equation 2-6

are not in good agreement with measured values in the vicinity of resonance. As discussed in Section 2.1.1, two representations of resistance of a resonator neck were employed in coupled resonator impedance calculations. The first assumes a resistance constant with frequency and in agreement with the measured data in the vicinity of resonance as shown in Figures 3-4 through 3-7. The second, considered as a further refinement and more representative of the data, is a point by point straight line fit through the actual data points. The results of using these two resistance models to calculate coupled resonator impedance are discussed in Sections 3.1.4 and 3.3, respectively. Suggestions for improvement of the resistance model are presented in Section 3.3.

The data in Figures 3-4, 3-5 and 3-6 represent repeat test runs spread over several days, and the spread in the data should be a good indication of repeatability of the measurements. Statistical calculations were performed on the data at each frequency point, and a typical value of the standard deviation estimate for a series of repeats is 10 percent of the mean for the resistance ( $\theta$ ). For the reactance ( $\chi$ ) the standard deviation is 0.1 dimensionless units.

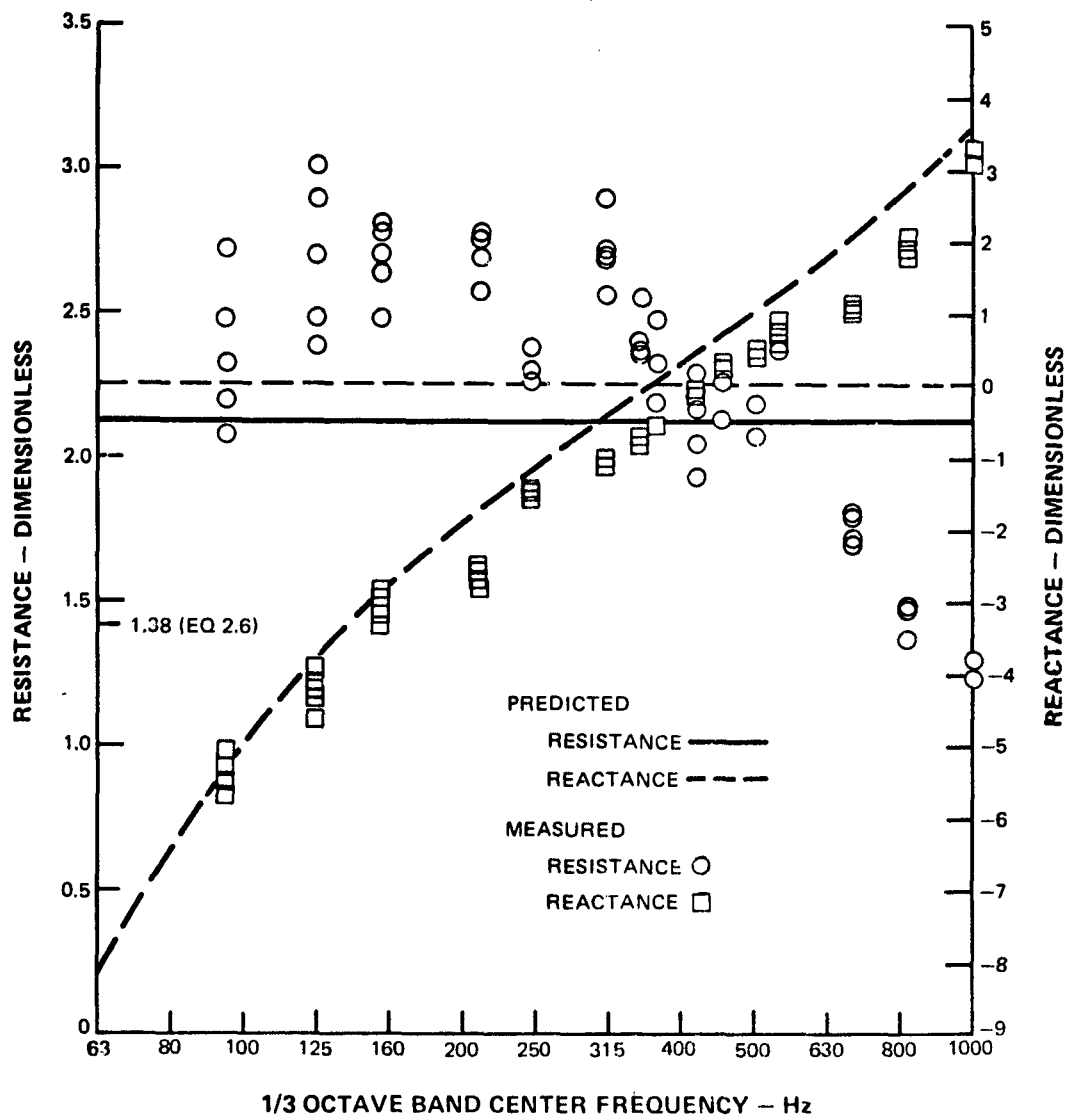


Figure 3-4 Comparison of Predicted and Measured Impedance, Resonator #1 at  $Mn = 0.45$

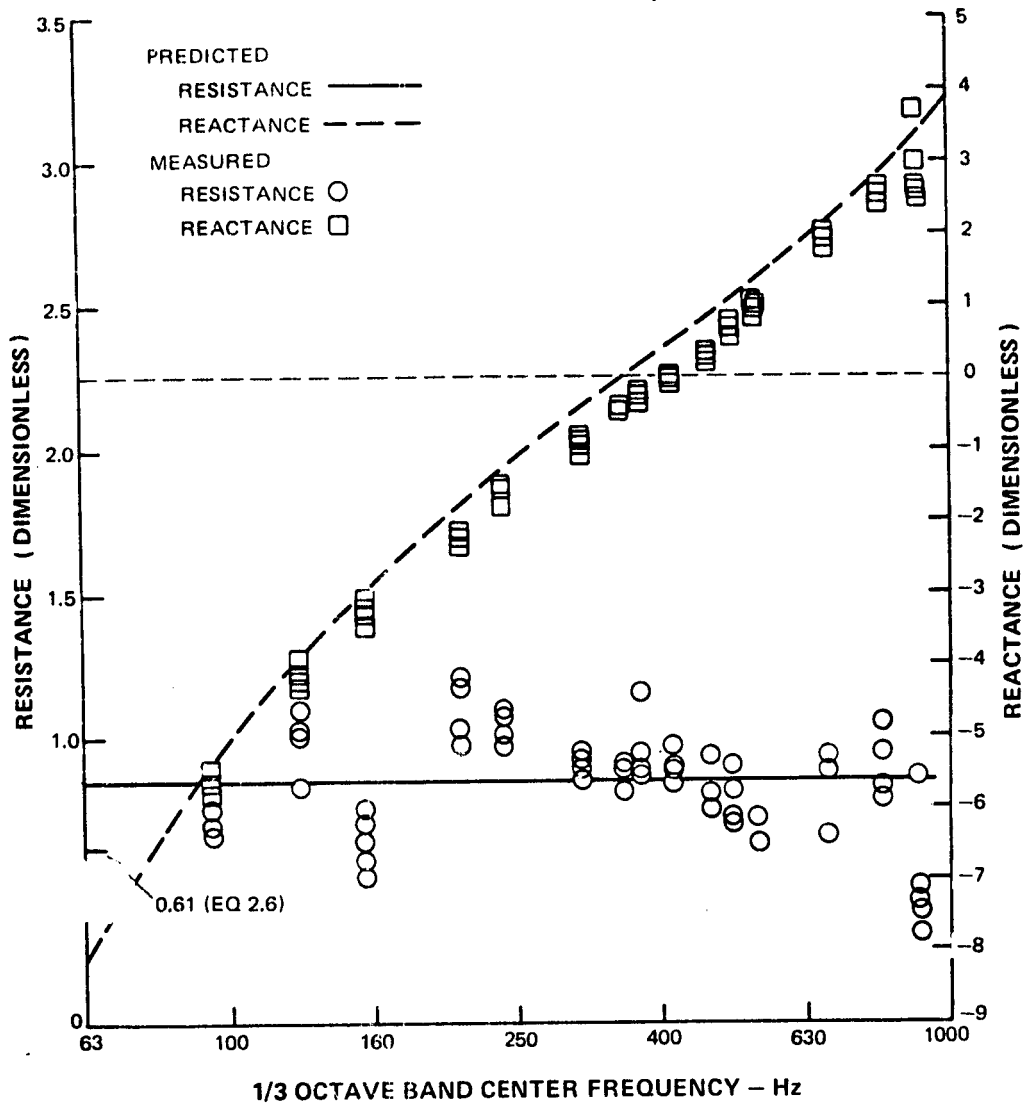


Figure 3-5 Comparison of Predicted and Measured Impedance, Resonator #2 at  $Mn = 0.45$

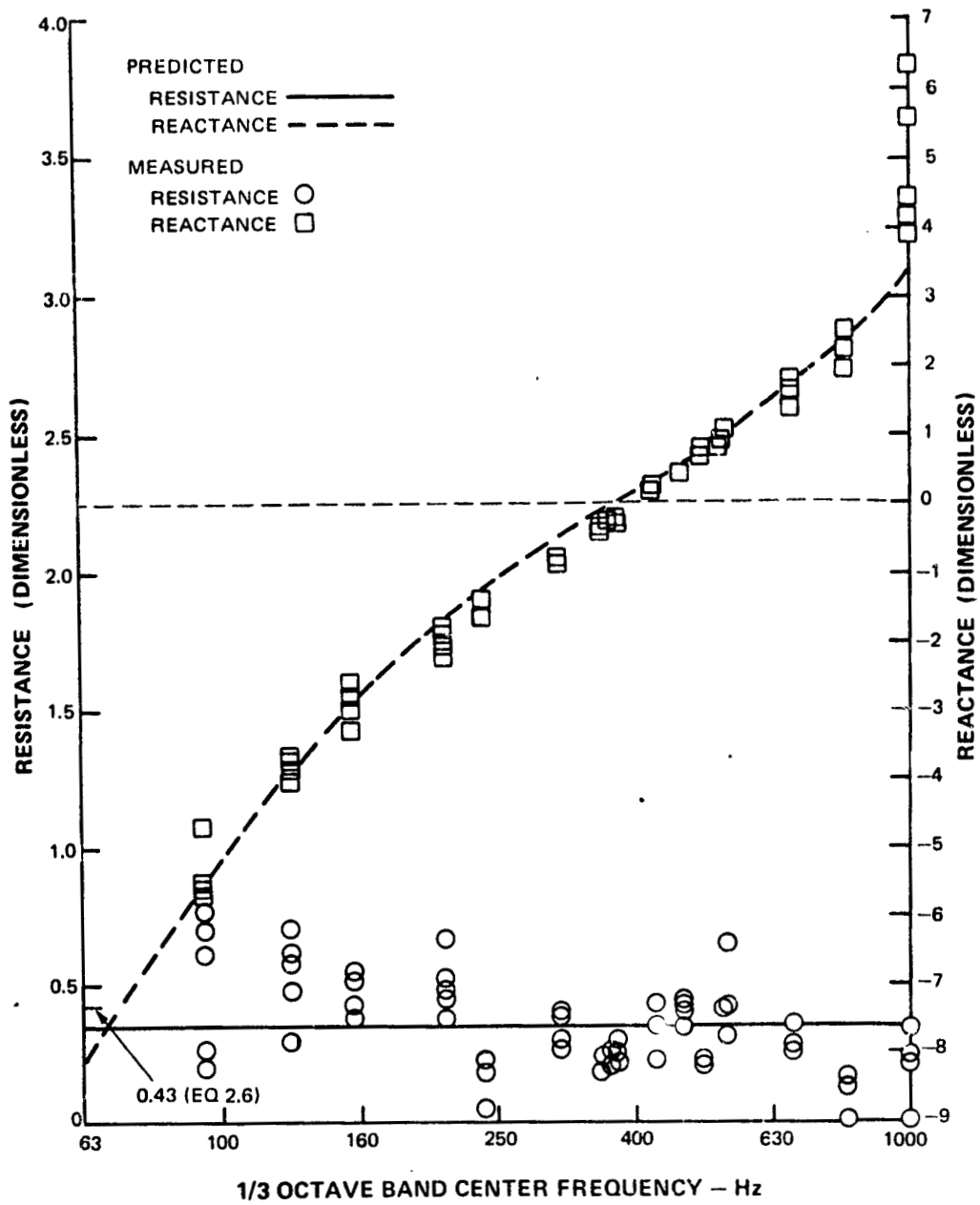


Figure 3-6 Comparison of Predicted and Measured Impedance, Resonator #3 at  $Mn = 0.45$

### 3.1.2.2. Effect of Grazing Flow

A comparison of single resonator model and measured impedance at a Mach number of 0.27 is presented in Figure 3-7. The results are similar to those at higher flow (Figures 3-4 through 3-7). The resistance again tends to decrease with increasing frequency, a phenomenon that is not understood but that can be seen in the results of other investigations<sup>(7)</sup>. At both flow Mach numbers, 0.27 and 0.45, the measured values of reactance of resonator # 1 are on average slightly less than the predicted values, indicating that the definitions of  $Ma$  and  $Ca$  in Equation 2-3 should be adjusted slightly for this configuration. This discrepancy between predicted and measured values is less for resonator # 2 (Figure 3-5) and disappears for resonator # 3 (Figure 3-6). Since the elements of the coupled resonators built and tested were similar in geometry to resonator # 3, and since equation 2-3 predicts the reactance well for this configuration, the equation was used without modification for definition of the coupled resonator parameters.

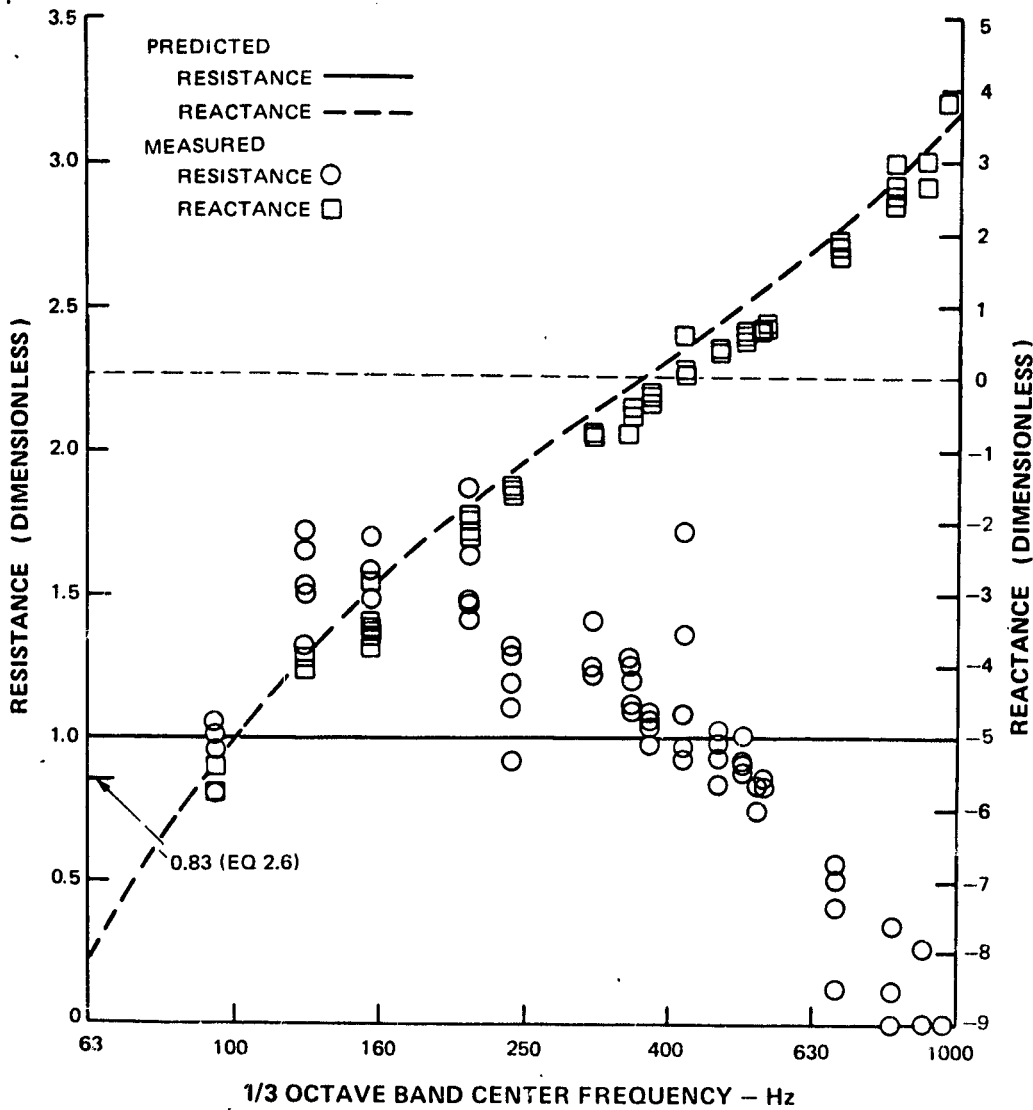


Figure 3-7 Comparison of Predicted and Measured Impedance, Resonator #1 at  $M_n = 0.27$

### 3.1.2.3 Effect of Sound Pressure Level

Changing sound pressure level was found to have no effect on impedance at grazing flows of Mach number 0.27 and 0.45. In designing the coupled resonators, therefore, sound pressure level was not a factor in determining geometrical parameters, such as length and diameter, of the necks exposed to flow. In addition, to make the parameters of the inner tube of each parallel coupled pair as nearly independent of sound pressure level as possible, a fibermetal insert was employed to set the resistance to the design value. The properties of fibermetals are relatively insensitive to sound pressure level compared to, for example, perforated plate<sup>(5)</sup>.

### 3.1.3 Coupled Resonator Impedance Measurements

The facility for measurement of coupled resonator impedance was identical to that for single resonators except that three microphone locations were required, as shown in Figure 3-8. As indicated in the figure, microphones were located in both cavities as well as in the duct wall. The cavity microphone signals are related to the net volume velocities into the two cavities by the equations:

$$P_2 = P_2 e^{i\omega t} e^{i\phi_1} = \frac{1}{C_1} \int (q_1 - q_3) dt = -\frac{i(q_1 - q_3)}{\omega C_1} \quad 3-4$$

$$P_3 = P_3 e^{i\omega t} e^{i\phi_2} = \frac{1}{C_2} \int (q_2 + q_3) dt = -\frac{i(q_2 + q_3)}{\omega C_2} \quad 3-5$$

and the impedance of the coupled resonator configuration is calculated from the relationship:

$$\dot{p}_1 = P_1 e^{i\omega t} \quad 3-6$$

$$Z_a = \frac{P_1}{q_1 + q_2} = \frac{-iP_1}{\omega C_1 P_2 e^{i\phi_1} + \omega C_2 P_3 e^{i\phi_2}} \quad 3-7$$

The various quantities are defined in Section 2.1 and in the list of abbreviations.

The pressure across the orifices exposed to grazing flow is not required in the calculations at this point, but can be expressed as:

$$P_1 - P_2 = M_1 \frac{dq_1}{dt} + R_1 q_1$$

or

$$P_2 - P_3 = M_2 \frac{dq_2}{dt} + R_2 q_2$$

which are consistent with equations 2-17 and 2-18 and Figures 2-3b and 3-8.

Three coupled resonator configurations tested were as described in Section 2.3, Table 2-VI, and the test conditions were identical to those for the three uncoupled resonators.

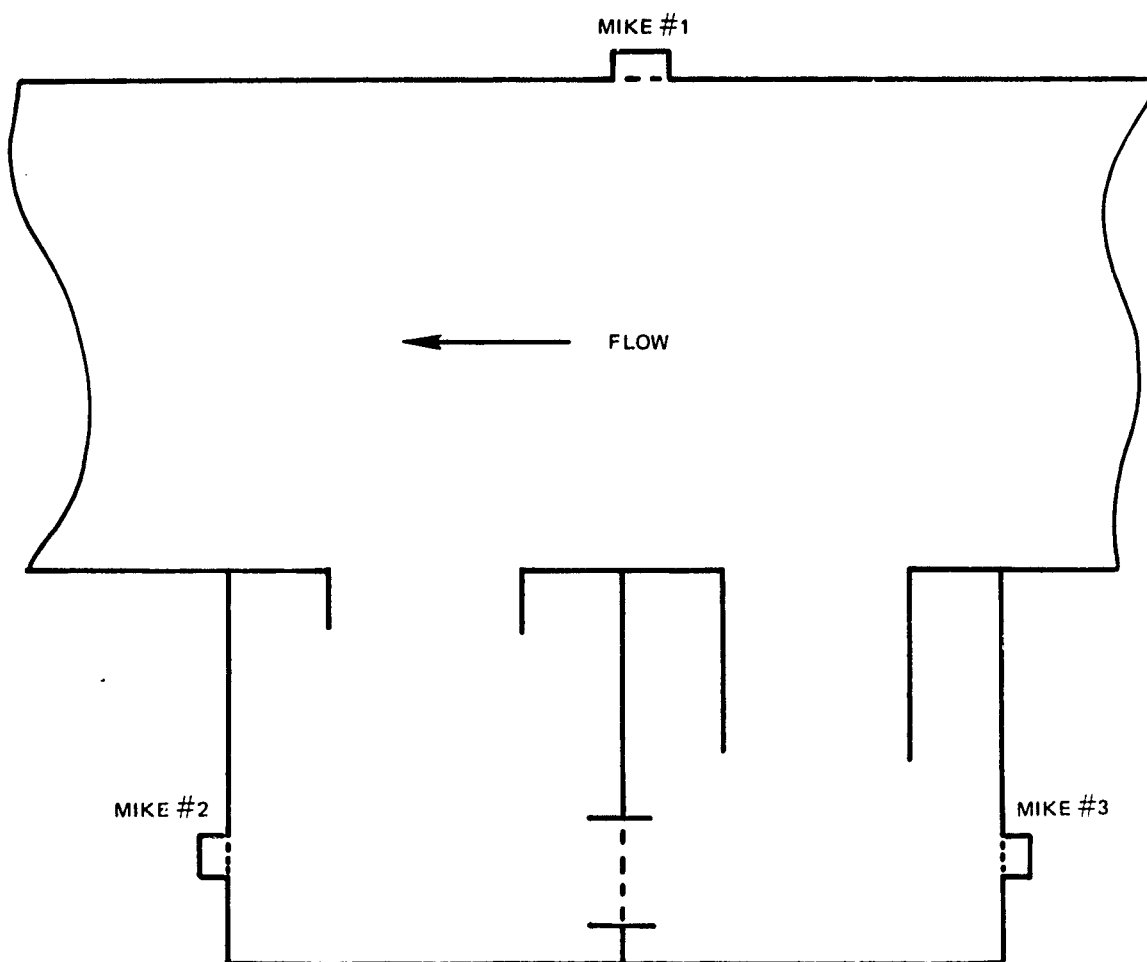


Figure 3-8 Microphone Placement for Coupled Resonator Impedance Measurements

### 3.1.4. Comparison of Coupled Resonator Impedance Measurements with Predicted Values

Examples of coupled resonator impedance measurements for the three coupled resonators at Mach number 0.45 grazing flow are presented in Figures 3-9, 3-10, and 3-11. All show the prediction inflection in the reactance characteristic discussed in Section 2.1. In the frequency range of the inflection, the predicted peak in the resistance is also seem to occur experimentally. As in the case of the single resonators, there is a tendency of resistance to decrease with frequency.

At the lower flow speed, similar results are obtained. Coupled resonator impedance measurements for the optimum configuration at Mach number 0.27 flow are presented in Figure 3-12. The same trend of resistance with frequency is observed in the figure as is observed at Mach number 0.45 flow.

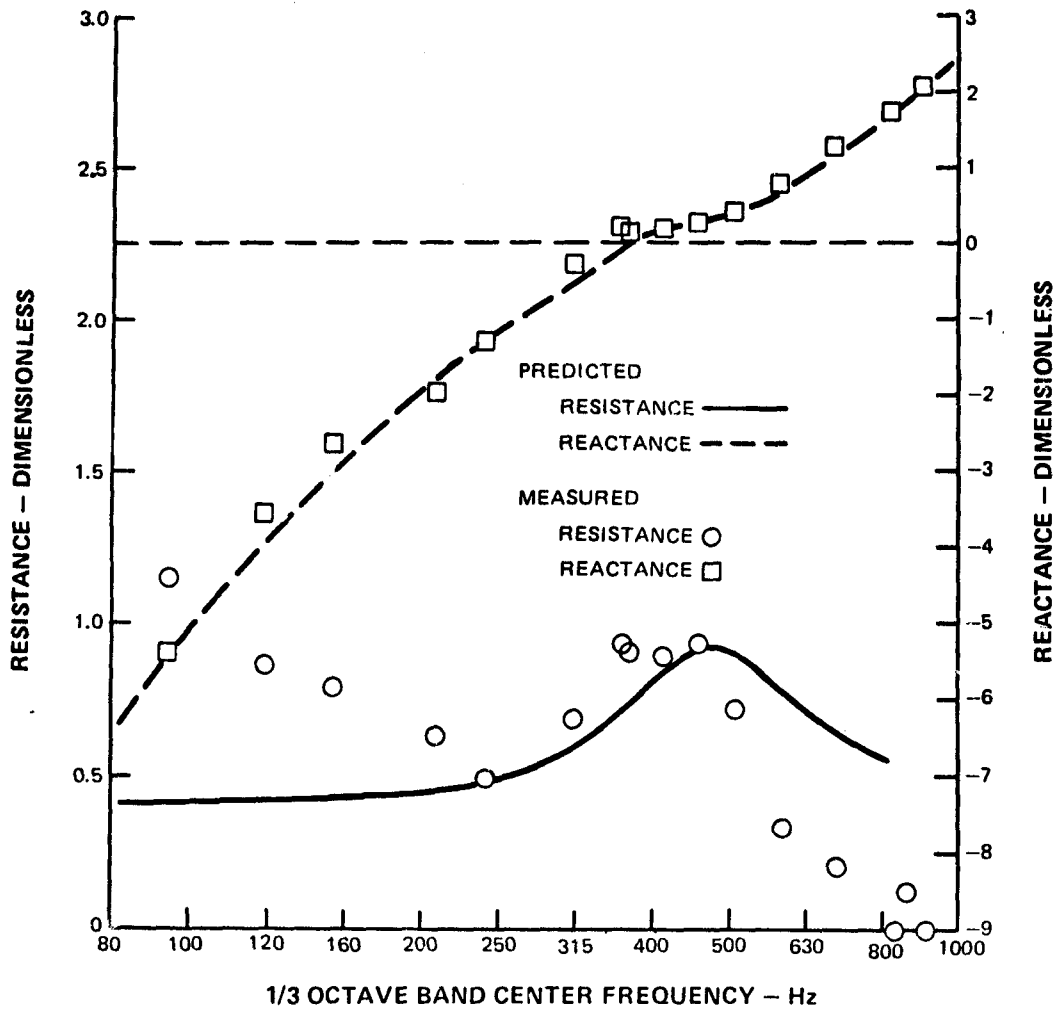


Figure 3-9 Comparison of Predicted and Measured Impedance, Off-Optimum A Coupled Resonator at  $Mn = 0.45$

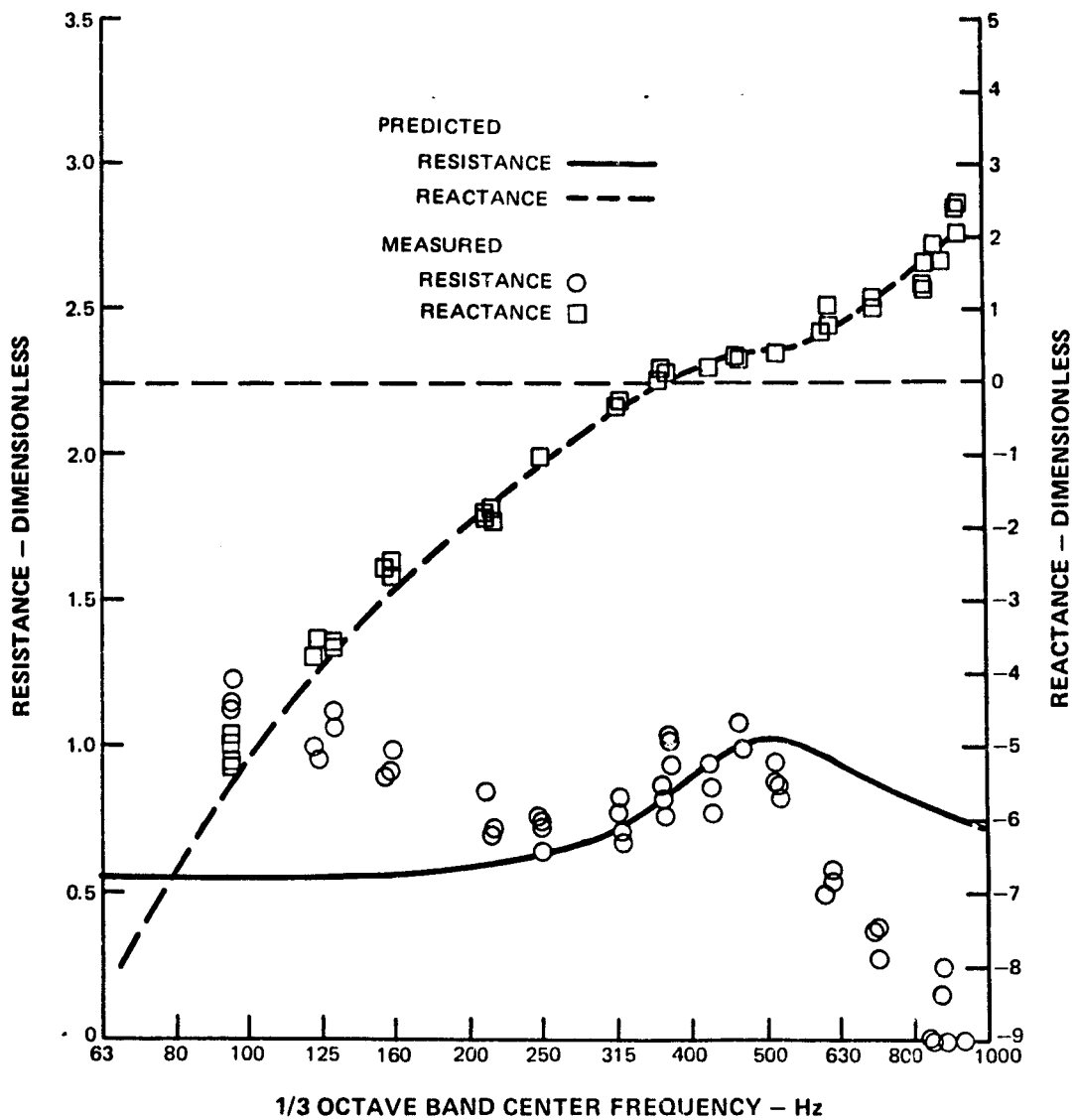


Figure 3-10 Comparison of Predicted and Measured Impedance, Optimum Coupled Resonator at  $M_n = 0.45$

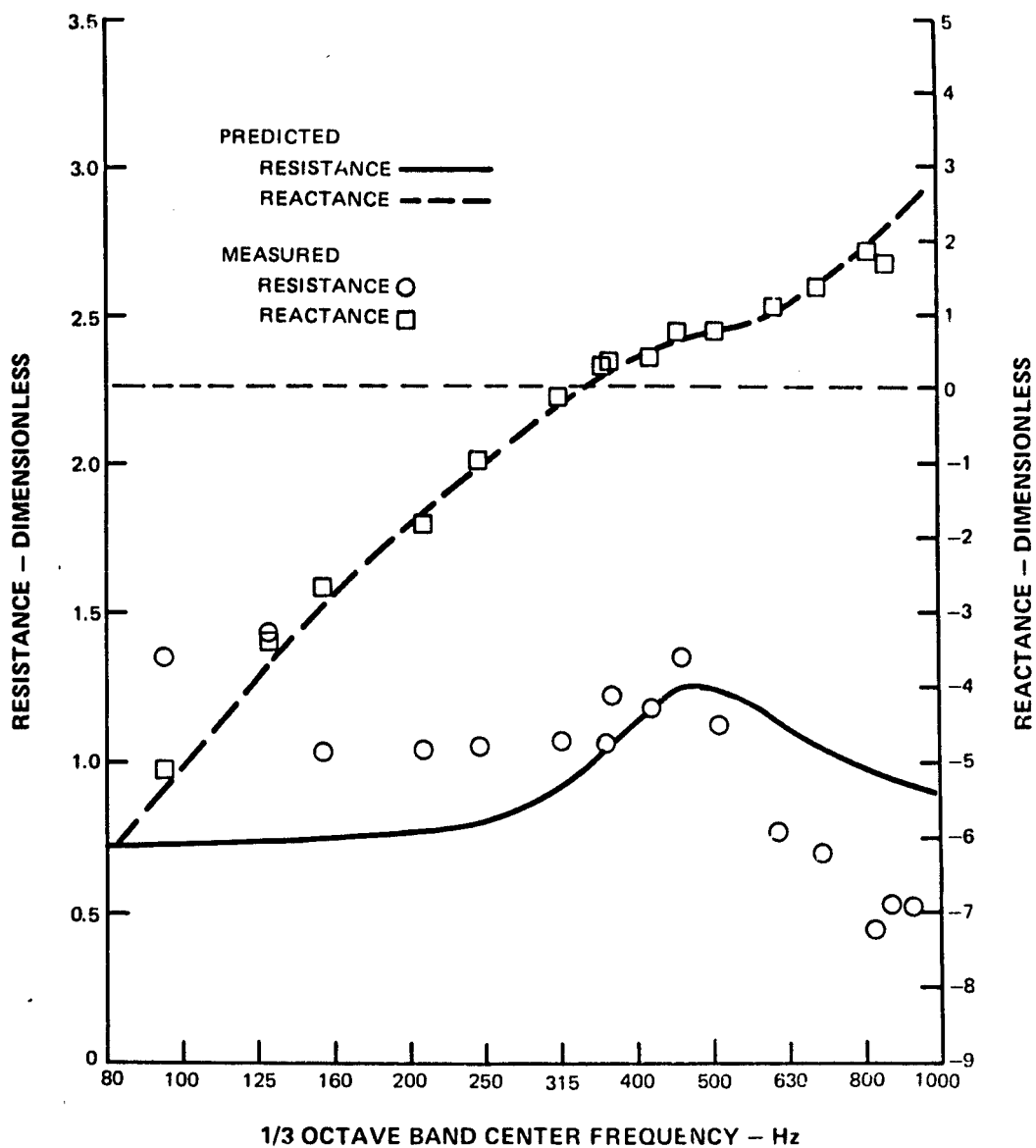


Figure 3-11 Comparison of Predicted and Measured Impedance, Off-Optimum B Coupled Resonator at  $M_n = 0.45$

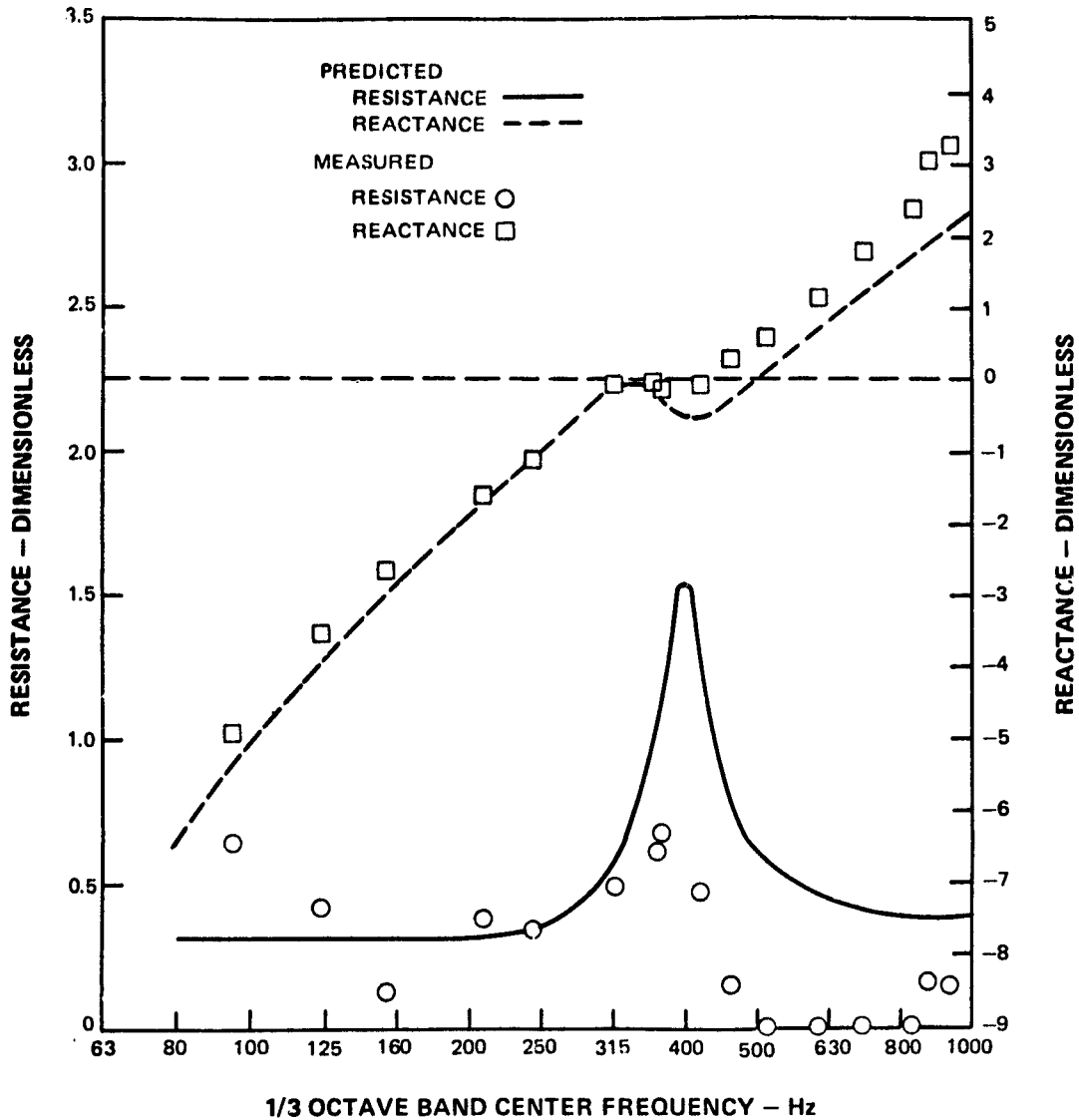


Figure 3-12 Coupled Resonator Impedance Data at  $Mn = 0.27$

The variation of resistance and reactance with frequency predicted from the model are included in the figures for comparison. The predicted reactance is in very good agreement with measured values. The predicted resistance does not display the decrease in value with increasing frequency. This latter discrepancy between prediction and measurement is believed to be the result of the use of a constant resistance in the modeling as is discussed further in Section 3.3.

In its general features, the modeling procedure is verified by the experimental measurements. Only the observed dependence of resistance on frequency remains to be investigated further.

## 3.2 COUPLED RESONATOR ATTENUATION TEST RESULTS

Panels of coupled resonators were fabricated for test according to the specifications of the optimum and two off-optimum configurations. In each case, the panel length, width, and depth were the same as for the P&WA baseline uncoupled panel. The test matrix was the same as that described for the impedance measurements. The noise source and measurement method were different, however, as described below.

### 3.2.1 Coupled Resonator Attenuation Test Facility

The flow duct described previously was used as a test facility for attenuation measurements. The noise source was broadband random in character. By recording and comparing the differences in one-third octave band levels in the two reverberation chambers, with a hardwall and a treated duct panel installed, attenuation levels were determined for the various test configurations.

### 3.2.2 Comparison of Predicted and Measured Attenuation of Coupled Resonator Panels

The attenuation of coupled resonator panels can be predicted using as input to the wave propagation computer program either the impedance predicted from the impedance models (Sections 2-1 and 2-2) or the impedance measured directly as described in Section 3-1. A comparison of these two prediction methods for the optimum coupled configuration is presented in Figure 3-13. Indications from this figure are that the two are in very good agreement. For comparison with test results, however, the measured impedance will be used.

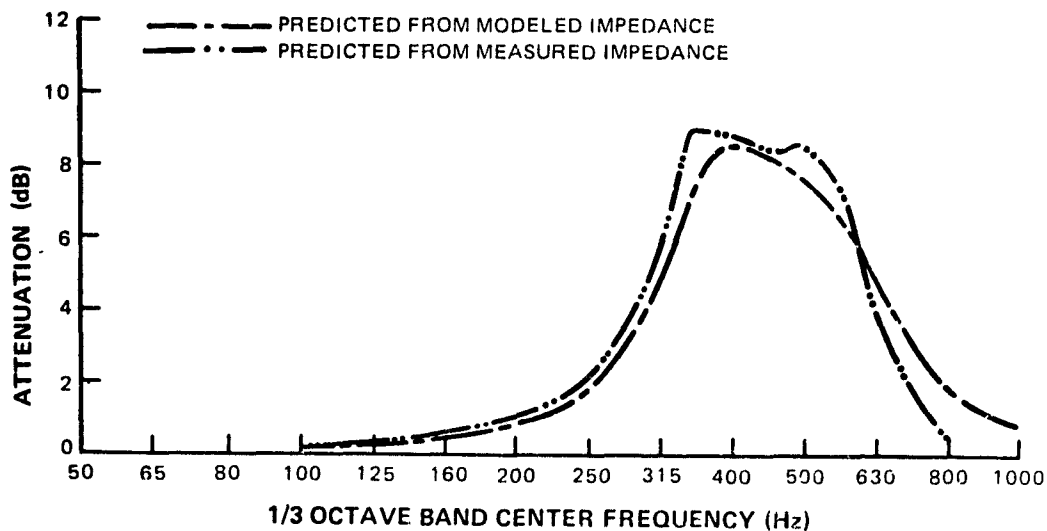


Figure 3-13 Comparison of Attenuation Predicted from Model and Measured Impedance, Optimum Configuration at  $M_n = 0.45$ , 50.8 cm Treatment Length

A comparison of the predicted and measured one-third octave band attenuation at  $Mn = 0.45$  for the three coupled configurations as a function of one-third octave band center frequency is presented in Figure 3-14. The agreement between the predictions and measurements is very good in the central one-third octave bands. The largest discrepancies are at the 250 and 630 Hz one-third octave band points. Because of the steepness of the curves near these two frequencies, only a slight shift in the curve of predicted attenuation to higher frequency would substantially improve the agreement. As predicted, the off-optimum A configuration shows the highest measured peak attenuation.

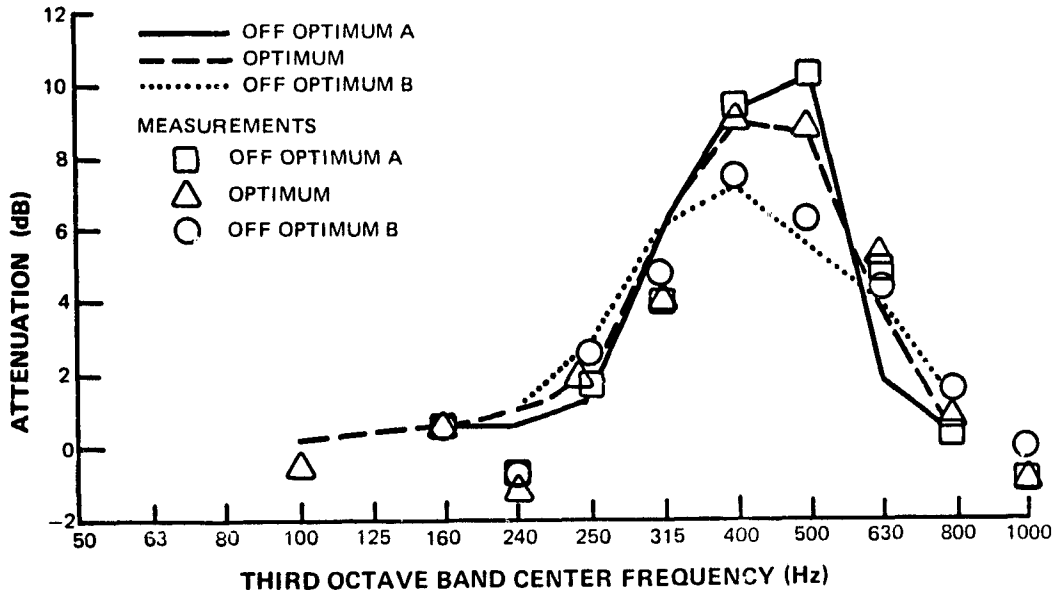


Figure 3-14 Comparison of Predicted and Measured Attenuation for Three Coupled Configurations,  $Mn = 0.45$ , 50.8 cm Treatment Length

A summary of calculations of source noise PNL reduction is presented in Table 3-II. Based on the attenuation measurements, all three coupled configurations give nearly equal PNL reductions. The average is about 5.1 PNdB as compared to 2.8 PNdB for the P&WA baseline and 3.8 PNdB for the improved baseline uncoupled configurations.

The closeness of the three coupled configurations on an annoyance (NOY) basis is shown in Figure 3-15 in which the attenuated source spectrum is plotted in annoyance units. As indicated in the figure, the controlling one-third octave bands are 315 and 800 Hz. Because of this, the comparison on a PNL basis depends critically on the attenuation in these bands, and as indicated in Figure 3-14, the three coupled configurations have nearly identical measured attenuations in these two bands. Despite this discrepancy between predicted and measured values, the overall agreement between predicted and measured attenuation is considered to be very good.

TABLE 3-II

SUMMARY OF RESONATOR ATTENUATION ON  
PNL BASIS, 0.8 CM LENGTH,  $M_n = 0.45$

<u>Configuration</u>	<u>NOYS</u>	<u>PNL</u>	<u><math>\Delta</math>PNL</u>
P&WA Baseline	43.0	94.3	2.8
Improved Baseline	40.1	93.3	3.8
Off Optimum A	36.9	92.0	5.1
Optimum	37.2	92.2	4.9
Off Optimum B	36.6	91.9	5.2

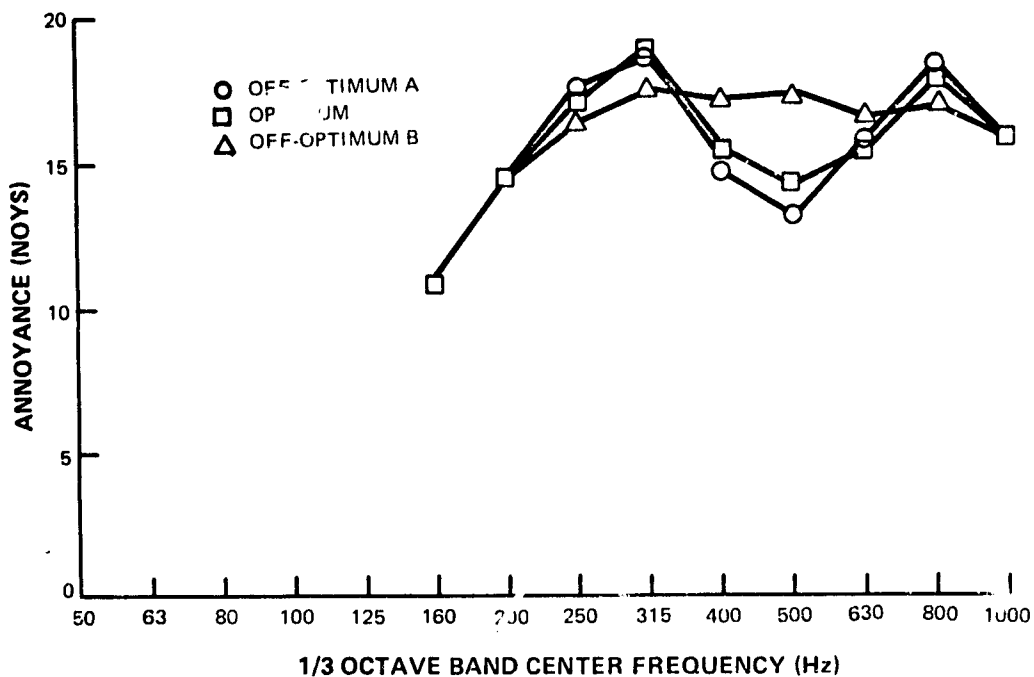


Figure 3-15 Comparison of Three Coupled Configurations on an Annoyance Basis

In Figure 3-16, the P&WA baseline measured attenuation data are compared with the measured values for the optimum coupled resonator. The results indicate that the coupling scheme in this case resulted in an increase in peak attenuation of about 50 percent and an increase in band-width of about one one-third octave band, as predicted in Section 2-4.

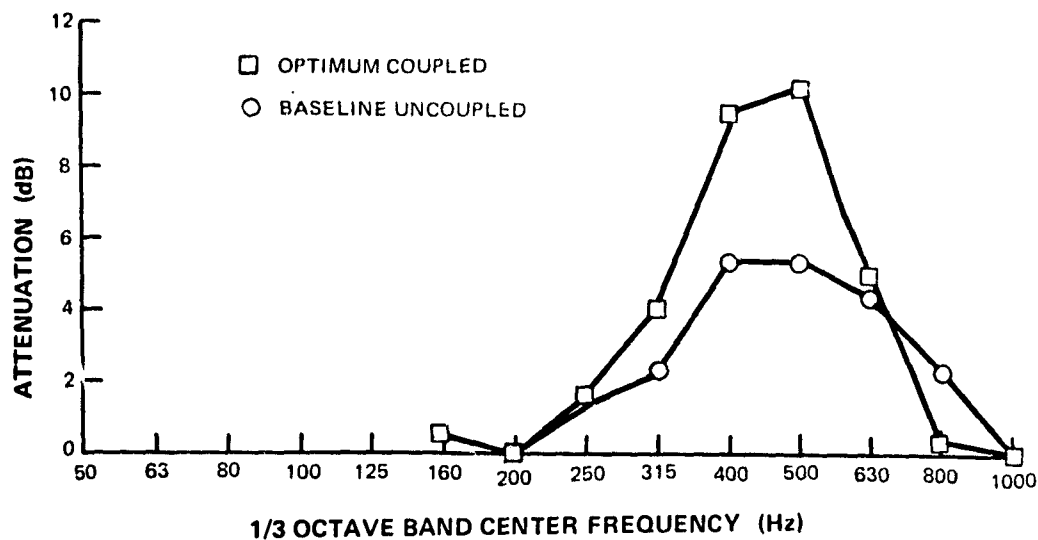


Figure 3-16 Comparison of Measured Attenuation for Baseline and Optimum Coupled Configuration at  $Mn = 0.45$ , 50.8 cm Treatment Length

### 3.3 Evaluation and Improvement of Resonator Models

The measured impedance of both single and coupled resonators is in good agreement with predictions, as indicated in Section 3.1, except for a tendency for measured resistance to decrease with increasing frequency. As indicated in Section 2.1, this behavior for single resonators is not consistent with the simple damped oscillator model, and to model a single resonator resistance varying with frequency requires the introduction of additional terms or variable coefficients into the governing equations. Furthermore, the physical significance of the parameters associated with these terms must be understood to derive the governing equations of coupled resonators. The measured behavior of resistance with frequency is not understood at this time and could well be the subject of additional studies. As was pointed out previously, however, similar trends in resistance as a function of frequency can be found in the results of other investigators<sup>(7)</sup>.

During the testing, measurements were made with the duct pressure microphone located on the orifice side of the flow duct near the orifice as well as in the location across the duct indicated in Figure 3-3. The two locations were found to be equivalent, and since the location of the duct microphone shown in the figure was more convenient, it was used throughout the testing.

With the assumption that the measured resistance is a property of the neck only, the impedance of the coupled resonators can be predicted from the measured impedance of single resonators of equal open area. This was done for the coupled resonators, and the results are presented in Figures 3-17, 3-18 and 3-19. In the figures, the impedance of the three parallel coupled configurations predicted from measured single resonator data are compared with measured values. The resulting agreement is good, and in general agreement with the concept of a resistance that is associated with resonator necks with grazing flow.

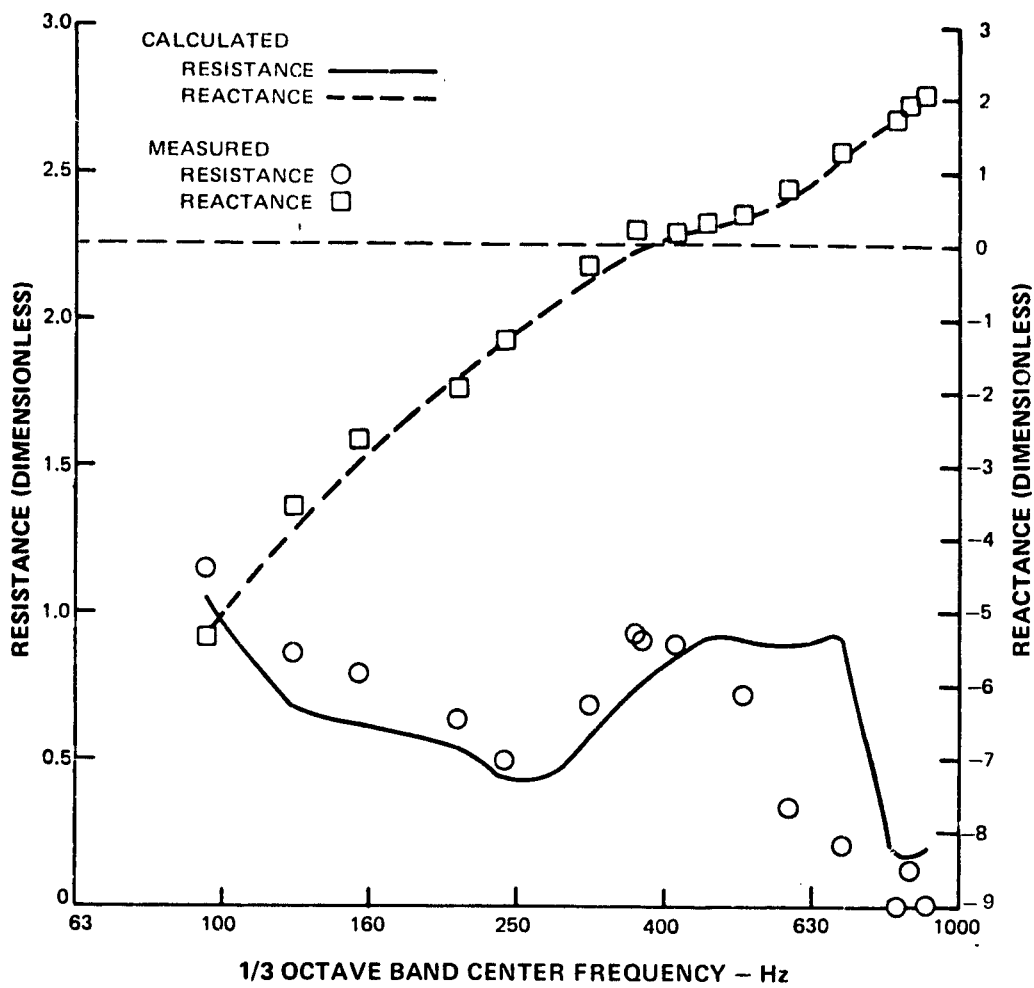


Figure 3-17 Comparison of Calculated and Measured Coupled Resonator Impedance, Off-Optimum  $A, M_n = 0.45$

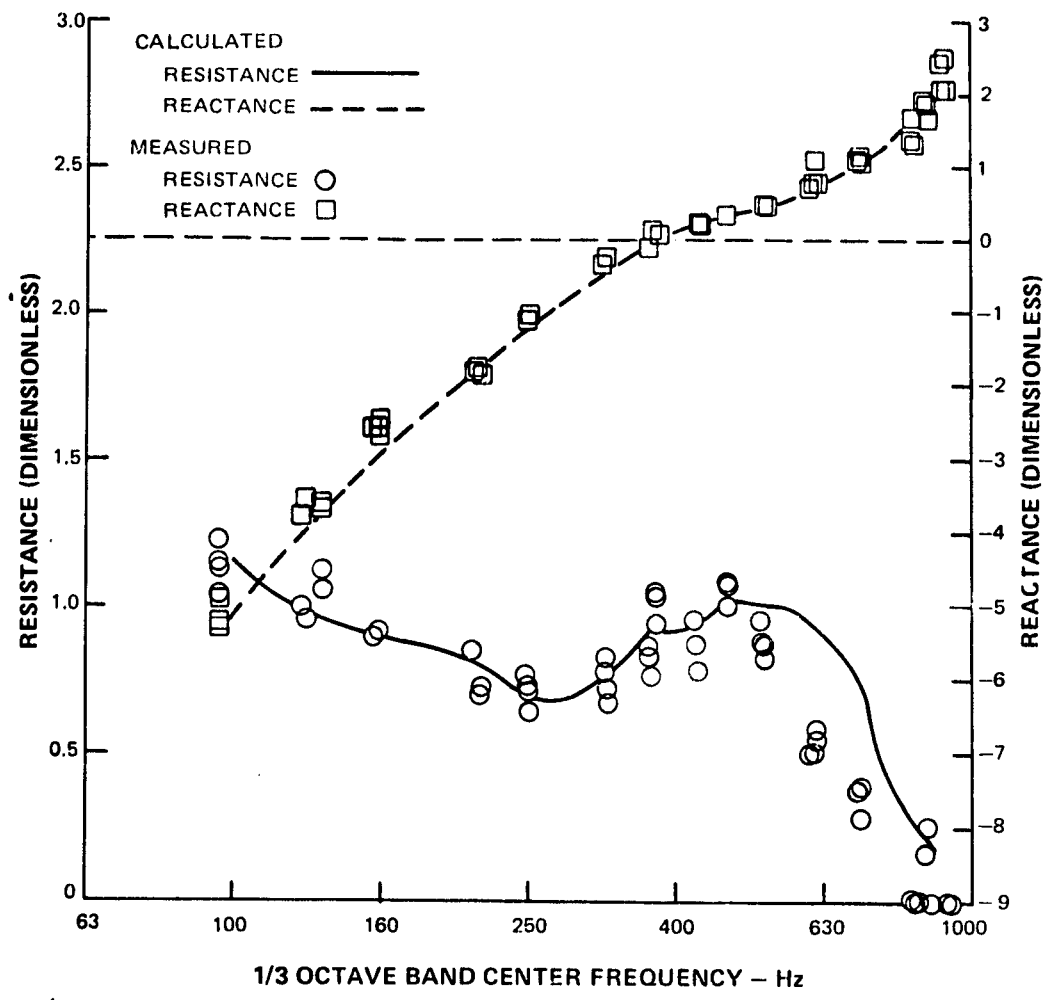


Figure 3-18 Comparison of Calculated and Measured Coupled Resonator Impedance, Optimum,  $M_n = 0.45$

REPRODUCTION OF THE ORIGINAL TABLE

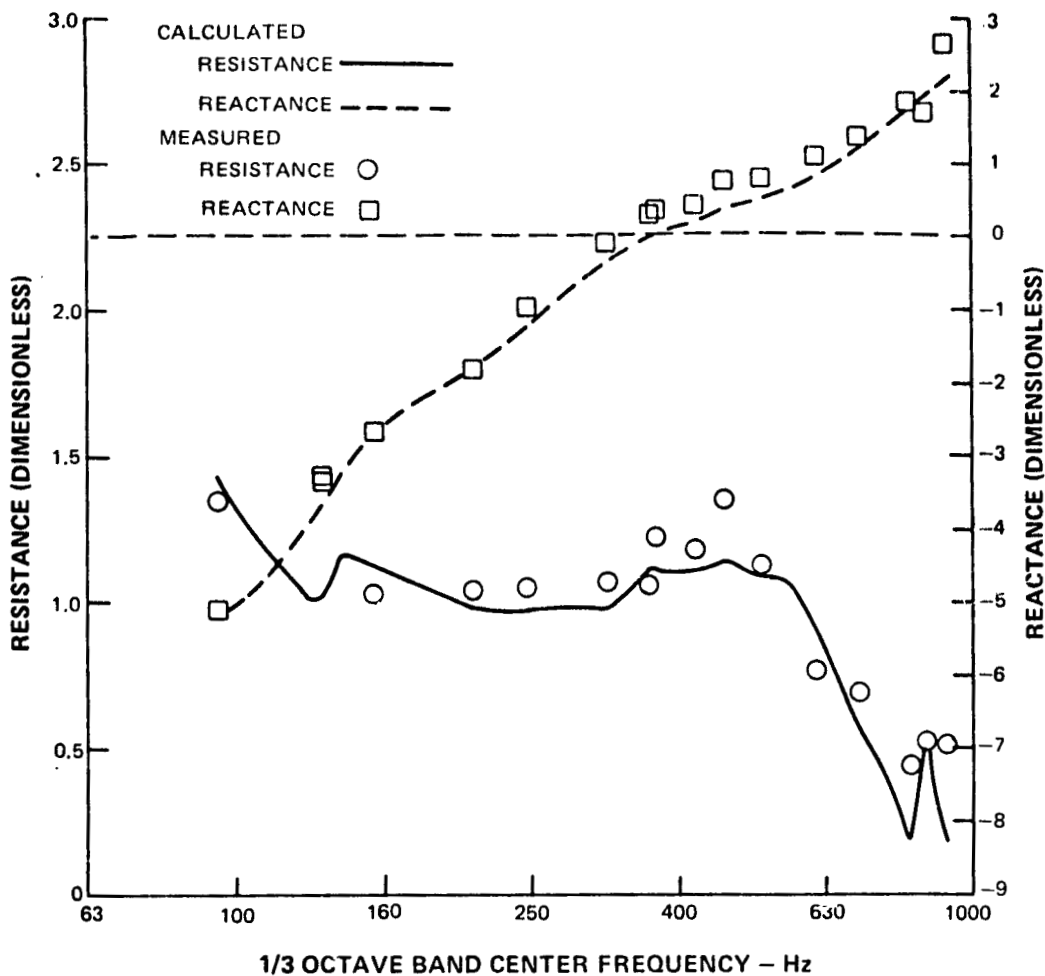


Figure 3-19 Comparison of Calculated and Measured Coupled Resonator Impedance, Off-Optimum B, Mn-0.45

### 3.4 EVALUATION OF THE COUPLED RESONATOR CONCEPT

The coupled resonator concept is evaluated on the basis of the PNL reduction of the source spectrum achieved, compared with the reduction that can be achieved by the uncoupled (baseline) resonators. As mentioned above, both coupled and uncoupled designs occupy equal volumes. Such a comparison indicates the degree of increase in liner effectiveness that can be achieved by the coupled scheme over the uncoupled.

The coupled resonators were found to be more effective than the uncoupled. Since the study involved coupling in pairs only, a natural question is what additional effectiveness could be achieved by the use of more complex coupling schemes. One calculation that can be performed without difficulty is the PNL reduction achieved by a hypothetical liner with

so many degrees of freedom that the impedance is optimum at every frequency. While such a liner might be impossible to construct, the calculated PNL reduction is a theoretical upper limit to the improvement that could be achieved by any scheme.

Plots of liners of constant attenuation against impedance for the least attenuated mode, such as Figure 2-5, indicate that the maximum possible attenuation for a 50.8 cm (20 inch) length is about 40 dB at low frequencies and nearly independent of frequency over the range of interest. This value was used to calculate the source spectrum PNL reduction, using the spectrum of Figure 2-7 without any noise floor, obtained from a many degree of freedom system, and in Figure 3-20 the reduction in PNL of the source spectrum is plotted as a function of  $1/n$ , where  $n$  is the number of degrees of freedom. The number of degrees of freedom of a resonator is taken to be equal to the number of equations of motion required to describe the system (i.e., the number of mass elements). The uncoupled resonator, therefore, has one degree of freedom, the series coupled has two, the parallel coupled has three, and the folded has five. As indicated in the figure, coupling resonators in pairs achieves only a small fraction of the theoretical potential, and the improvement should increase rapidly at some point as the number of resonators coupled together is increased.

In Figure 3-20, two configurations tested are indicated by the squares. These correspond to the uncoupled baseline configuration ( $n = 1$ ) and the optimum parallel coupled configuration ( $n = 3$ ). It is assumed that an infinite number of degrees of freedom should be assigned to the hypothetical ideal liner, discussed above, that gives the maximum possible attenuation of the source spectrum at every frequency, and the resulting calculated PNL reduction is indicated by a circle. The dashed line is used to indicate the increase in source noise attenuation with increasing degrees of freedom that must occur as the characteristics of the hypothetical ideal liner are approached. As shown in Table 3-II the parallel coupled resonator is significantly more effective in reducing the source spectrum noise than the uncoupled. Figure 3-20 indicates, however, that a much greater potential for improvement exists if the characteristics of the ideal liner can be approached more closely. Further study is required to determine to what extent this can be accomplished.

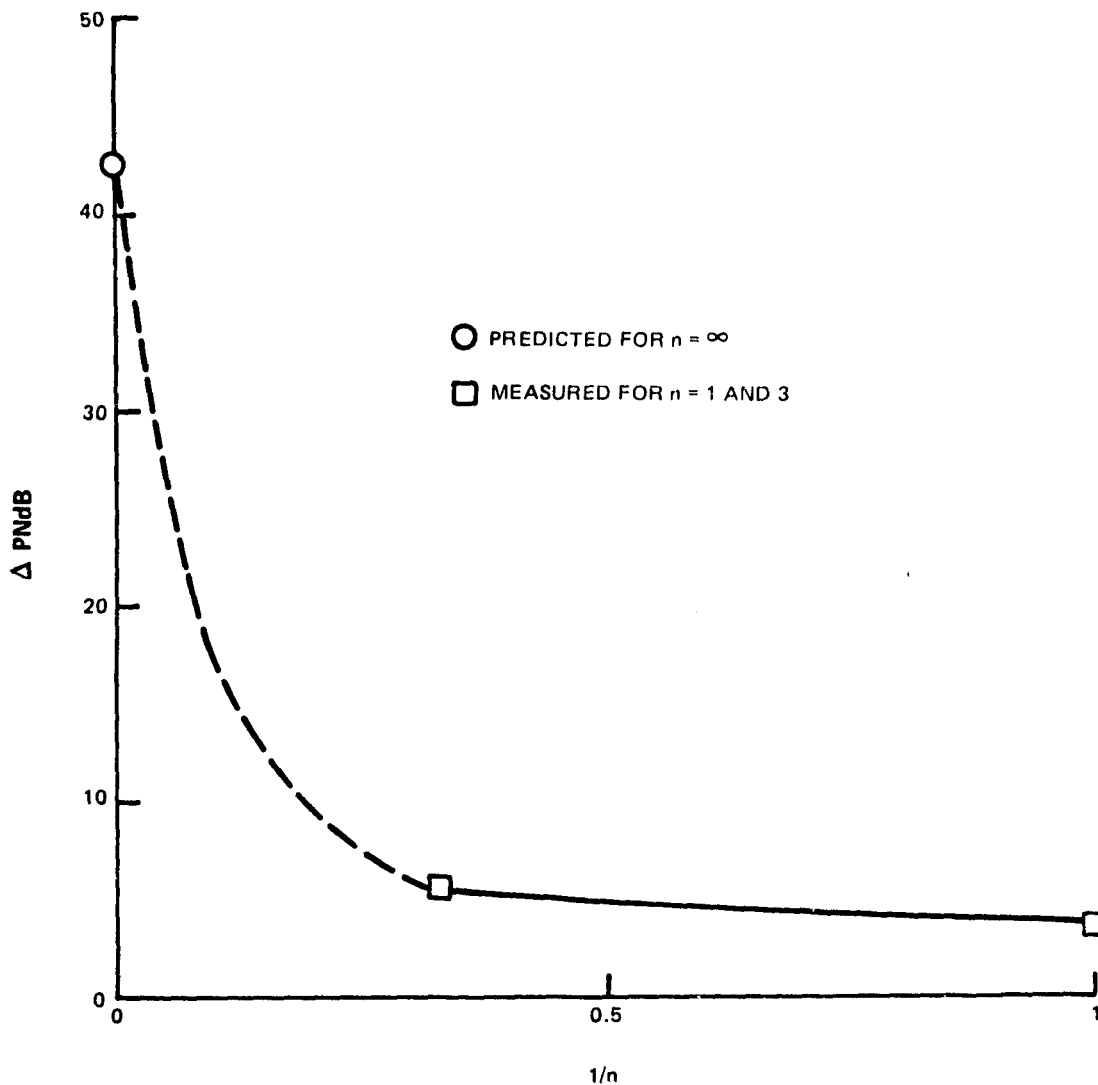


Figure 3-20 Source Spectrum PNL Reduction Versus Reciprocal of Degrees of Freedom

### 3.4.1 Evaluation on Basis of Alternate Criterion

As discussed in Section 2.2, an alternate criterion is the minimum length of liner required to achieve a given PNL reduction. Such a criterion would be applicable to specific turbofan engine design problems.

Studies were conducted to determine the length of coupled liner required to achieve the same PNL reduction of the source spectrum as 50.8 cm. of the baseline liner. In Table 3-III, equivalent lengths of liner are listed. As indicated in the table, the optimum parallel coupled configuration is predicted to have an equivalent length 24% less than the baseline.

By all indications, the coupled resonator approach shows considerable promise as a means for increasing treatment effectiveness at low frequency in terms of increased attenuation for a given length of liner and reduced liner length to achieve a given attenuation with respect to a broadband source spectrum, such as that considered in this study. Indications are that much greater increase in effectiveness could be achieved by more complex coupling schemes.

TABLE 3-III

EQUIVALENT LENGTHS OF BASELINE AND COUPLED  
LINERS FOR SOURCE REDUCTION OF 3.8 PNdB, MN = 0.45

<u>Configuration</u>	<u>Equivalent Length, cm</u>	<u>% Decrease</u>
Improved Baseline	50.8	-0-
Optimum Coupled	38.6	24

## 4.0 CONCLUSIONS AND RECOMMENDATIONS

### 4.1 CONCLUSIONS

1. Investigations were conducted of impedance characteristics of single uncoupled Helmholtz resonators subjected to grazing flow and have shown that existing models for the parameters of the governing equations, in terms of resonator geometry, are satisfactory except for an unexplained decrease in resistance with increasing frequency.
2. Impedance models were derived for three types of coupled resonators based on the governing equations of motion and the single resonator equation parameters. Good agreement between predicted and measured impedance was obtained using measured values of the single resonator parameters, including the observed dependence of resistance on frequency.
3. By a suitable choice of parameters, the coupled resonator impedance could be adjusted so that a more nearly optimum resistance and reactance could be achieved over a wider range of frequency compared to the uncoupled resonator.
4. Coupled resonator attenuation predictions were made for the frequency range 50 to 1000 Hz using the impedance models with an existing wave propagation computer program. Predicted and measured attenuation were in very good agreement, and predicted improvement in attenuation obtained by use of coupled resonators compared to the uncoupled resonators were verified.
5. The measured improvement in attenuation, under the optimization constraints used, of low frequency sound achieved by the best coupled scheme over the best uncoupled was a simultaneous increase in peak attenuation of 50% and in attenuation bandwidth of 1/3 octave.

### 4.2 RECOMMENDATIONS

1. Further experimental and analytical work is required to verify and to model the observed decrease of Helmholtz resonator resistance with increasing frequency.
2. For purposes of low frequency sound absorber design in a turbofan engine exhaust environment, the capability to model resonator parameters should be extended to include velocities to  $M_n = 0.65$  and a wider range of resonator neck geometry.
3. Although results obtained to date by coupling resonators in pairs show good improvement over uncoupled design, considerable potential for further improvement without increase in treatment volume still exists (see Figure 3-20). Studies are required to evaluate extension of the coupling scheme to larger numbers of resonators to achieve as much as possible of this potential within practical construction limitations.

## LIST OF SYMBOLS

$a_1$	empirical constant
$A_h$	resonator neck area ( $\text{cm}^2$ )
$A_s$	resonator surface area ( $\text{cm}^2$ )
$c$	speed of sound ( $\text{cm}/\text{sec}$ )
$C_a, C_i$	analogous compressibility ( $\text{cm}^2\text{sec}/\text{cgs Rayl}$ )
$d$	resonator neck diameter ( $\text{cm}$ )
$i$	$\sqrt{-1}$
$l$	resonator neck length ( $\text{cm}$ )
$l_e$	effective resonator neck length ( $\text{cm}$ )
$M, Mn$	Mach number
$M_a, M_i$	analogous mass ( $\text{cgs Rayls}/\text{cm}^2 \text{ sec}$ )
$p$	acoustic pressure ( $\text{dynes}/\text{cm}^2$ )
$P$	amplitude of $p$ ( $\text{dynes}/\text{cm}^2$ )
$q$	acoustic volume velocity ( $\text{cm}^{-1} \text{ sec}^{-1}$ )
$Q$	amplitude of $q$ ( $\text{cm}^{-1} \text{ sec}^{-1}$ )
$R_a, R_i$	analogous resistance ( $\text{cgs Rayls}/\text{cm}^2$ )
$V$	resonator volume ( $\text{cm}^3$ )
$X_a$	analogous reactance ( $\text{cgs Rayls}/\text{cm}^2$ )
$Z$	impedance ( $\text{cgs Rayls}$ )
$Z_a$	analogous impedance ( $\text{cgs Rayls}/\text{cm}^2$ )
$\zeta$	specific acoustic impedance
$\theta$	specific acoustic resistance
$\rho_0$	ambient density ( $\text{gm}/\text{cm}^3$ )
$\sigma$	$A_h/A_s$
$X$	specific acoustic reactance ( $\text{cgs Rayls}/\text{cm}^2$ )
$\omega$	angular frequency ( $\text{sec}^{-1}$ )

## REFERENCES

1. D. C. Mathews and A. A. Peracchio, "Progress in Core Engine and Turbine Noise Technology", AIAA Paper No. 74-948, August 1974.
2. (No author) "Study and Development of Turbofan Nacelle Modifications to Minimize Fan-Compressor Noise Radiation, Volume IV - - Flightworthy Nacelle Development", NASA CR-1714, January 1971.
3. E. L. Zwieback, et. al., "Investigation of DC-8 Nacelle Modifications to Reduce Fan-Compressor Noise in Airport Communities, Part IV - - Flight Acoustical and Performance Evaluations", NASA CR-1708, December, 1970.
4. P. M. Morse, Vibration and Sound, 2nd ed, McGraw-Hill (1948).
5. E. Feder and L. W. Dean, "Analytical and Experimental Studies For Predicting Noise Attenuation in Treated Ducts For Turbofan Engines," NASA CR-1373 (1969).
6. U. Ingard and H. Ising, "Acoustic Non-Linearity of an Orifice," J. Acoust. Soc. Am., 42, pp. 6-17, (1967).
7. H. E. Plumblee, et. al., "Sound Propagation In and Radiation From Acoustically Lined Flow Ducts: A Comparison of Experiment and Theory", NASA CR-2306, October, 1973.
8. P. M. Morse and U. Ingard, Theoretical Acoustics, pp. 708 - 714, McGraw-Hill (1968).